



FACULTY OF SCIENCE
Charles University

MASTER THESIS

Bc. Anna Agafonova

**Relationship between travelling waves
on the surface and neural activity inside
the cat primary visual cortex**

Department of Cell Biology

Supervisor of the master thesis: Karolína Korvasová, M.Sc., Ph.D.

Study programme: Bioinformatics

Study branch: Bioinformatics

Prague 2023

Prohlašuji, že jsem tuto diplomovou práci vypracoval(a) samostatně a výhradně s použitím citovaných pramenů, literatury a dalších odborných zdrojů. Tato práce nebyla využita k získání jiného nebo stejného titulu.

Beru na vědomí, že se na moji práci vztahují práva a povinnosti vyplývající ze zákona č. 121/2000 Sb., autorského zákona v platném znění, zejména skutečnost, že Univerzita Karlova má právo na uzavření licenční smlouvy o užití této práce jako školního díla podle §60 odst. 1 autorského zákona.

V dne
Podpis autora

I would like to express my huge gratitude for the support and guidance from my supervisor Karolína Korvasová, M.Sc., Ph.D.. I deeply appreciate all of the time she dedicated to assisting me with data analysis, explaining to me fundamentals or just having discussions about neuroscience with me. Moreover, I am deeply thankful for her role as an inspiring example of a woman in science.

My thanks also extend to the Computational Systems Neuroscience Group (CSNG) for their efforts in organizing great seminars and courses on Computational Neuroscience that kept me motivated and inspired to pursue studying neuroscience.

Furthermore, I extend my appreciation to Diego Contreras at the University of Pennsylvania for providing me with the recordings that I analyzed.

Title: Relationship between travelling waves on the surface and neural activity inside the cat primary visual cortex

Author: Bc. Anna Agafonova

Department: Department of Cell Biology

Supervisor: Karolína Korvasová, M.Sc., Ph.D., Department of Software and Computer Science Education

Abstract: Large population events such as up states, oscillations and travelling waves are ubiquitously observed in recordings from the surface of the brain such as electroencephalography (EEG) or electrocorticography (ECoG). However, our ability to interpret these events is limited by our lack of understanding of their cellular origin. For instance, it is not known whether the population events on the cortical surface influence the activity across the entire cortical column or whether their impact is limited to the upper cortical layers. Further, the surface population events may exhibit themselves in the form of oscillations at different frequency bands, possibly specific to certain cortical layers. The aim of this thesis is to describe neural activity in the entire cortical column during the surface events and investigate how it differs from the rest. Particularly, we investigated the level of local field potential cross-correlations and the structure of the power spectrum across the depth of the cortical column of a cat and compared the results during up states vs. down states as measured on the cortical surface. We found that the local field potential measured in the depth of the cortex is more correlated to the ECoG recording during down states compared to up states. During up states, the signals showed increased power at all frequencies, probably reflecting increased synaptic input and the resulting neural activity. In the primary visual cortex, we observed prominent peaks at 20Hz in higher cortical layers and peaks with 30Hz frequency in the deep layers.

Keywords: primary visual cortex, travelling waves, brain waves

Contents

1	Introduction	2
1.1	A History Of Neuroscientific Discoveries	2
1.2	Local Field Potentials	2
1.3	Brain Waves	4
1.4	Effects of Anaesthesia on Brain Oscillatory Patterns	7
1.5	On the Anatomy of Primary Visual Cortex	7
1.6	Why to Study Brain at Rest?	8
1.7	The Objective of the Thesis	9
2	Methodology	11
2.1	Experimental Setup	11
2.2	Data Preprocessing	11
2.3	A Method for Analyzing Surface Events	13
2.3.1	Exploration of Travelling Waves and Motivation for Up States	13
2.3.2	Details on Up State & Down State Definition	13
2.4	Signal to Signal Correlation	16
2.5	Spectral Analysis	16
2.6	Statistical Testing	17
3	Results	19
3.1	Correlation Analysis of ECoG and laminar Probe Signals	19
3.2	Spectral Analysis of Neural Activity During Up States and Down States	21
3.2.1	Periods of Surface Up States are Characterized by Higher Overall Total Power	21
3.2.2	The Activity is Dominated by the Alpha and Beta Bands and Demonstrates Depth-Related Variability	23
3.3	Travelling Waves	25
4	Discussion	29
	Conclusion	31
	Bibliography	32
	List of Other Resources	37
	List of Figures	38
	List of Abbreviations	43
A	Attachments	44
A.1	First Attachment	44
A.2	Second Attachment	44
A.3	Third Attachment	44

1. Introduction

1.1 A History Of Neuroscientific Discoveries

For a very long time, in the history of neuroscience, our understanding of the brain was limited to mere observation. The earliest discoveries heavily relied on dissections. While it contributed significantly to our knowledge of the brain's anatomy and laid a strong foundation for modern experiments, it did not explain what exactly the brain does. An example of such efforts is the work of Andreas Vesalius in "On the Fabric of the Human Body," which rigorously mapped the brain's structures during the 16th century. Yet it did not automatically lead to accurate conclusions about brain function. At that time, the prevailing belief was that the brain serves as a "spirit" container, and nerves transported this "spirit" throughout the body (Abbott, 2015).

To deepen our understanding of brain function, researchers had to rely on studying brain lesions. One famous case is that of Phineas Gage, a 19th-century railway worker who survived a severe accident, which caused significant brain damage in the area of the prefrontal cortex. Remarkably, Gage retained his intellectual abilities but experienced a drastic change in morality, leading to descriptions of him as irresponsible, unreliable, and rude. This unfortunate accident taught neuroscience how vital the prefrontal cortex is for human social behaviour (Jennings, 1999).

Centuries of lesion research have yielded a functional map of the brain. Yet, a breakthrough came with the advancement in physics, specifically in electricity. In 1924, Hans Berger discovered electrical brain activity using scalp electrodes, leading to the establishment of electroencephalography (EEG) as a method for studying brain activity (Berger, 1938). Subsequently, scientists learned to use intracranial electrodes to measure electrical activity from within the brain. Thus, modern neuroscience has made significant progress, unveiling the true nature of the "spirit" as electrical signals that not only travel through the body but also activate muscles, allowing movement, breathing, and function.

Today, sophisticated arrays of electrodes are employed to measure signals from multiple sites simultaneously. The obtained signal is divided into two components: low frequency (below 500 Hz), summarizing collective activity within an area, and high frequency (above 500-1000 Hz), referred to as multiunit activity (MUA) (Burns et al., 2010). MUA measurements are easier to interpret since they represent the spiking activity of a small number of neurons within a specific region. The spike, or action potential (AP), constitutes the fundamental electrical activity of single neurons. It is a rapid and reversible change in the electrical potential across the cell membrane of a neuron, allowing for the transmission of signals along the nerve cell.

1.2 Local Field Potentials

The electrophysiological signal constitutes low- and high-frequency components. However, in this work, we focused on the low-frequency component acquired from intracranial and surface electrodes, commonly known as the local field potential

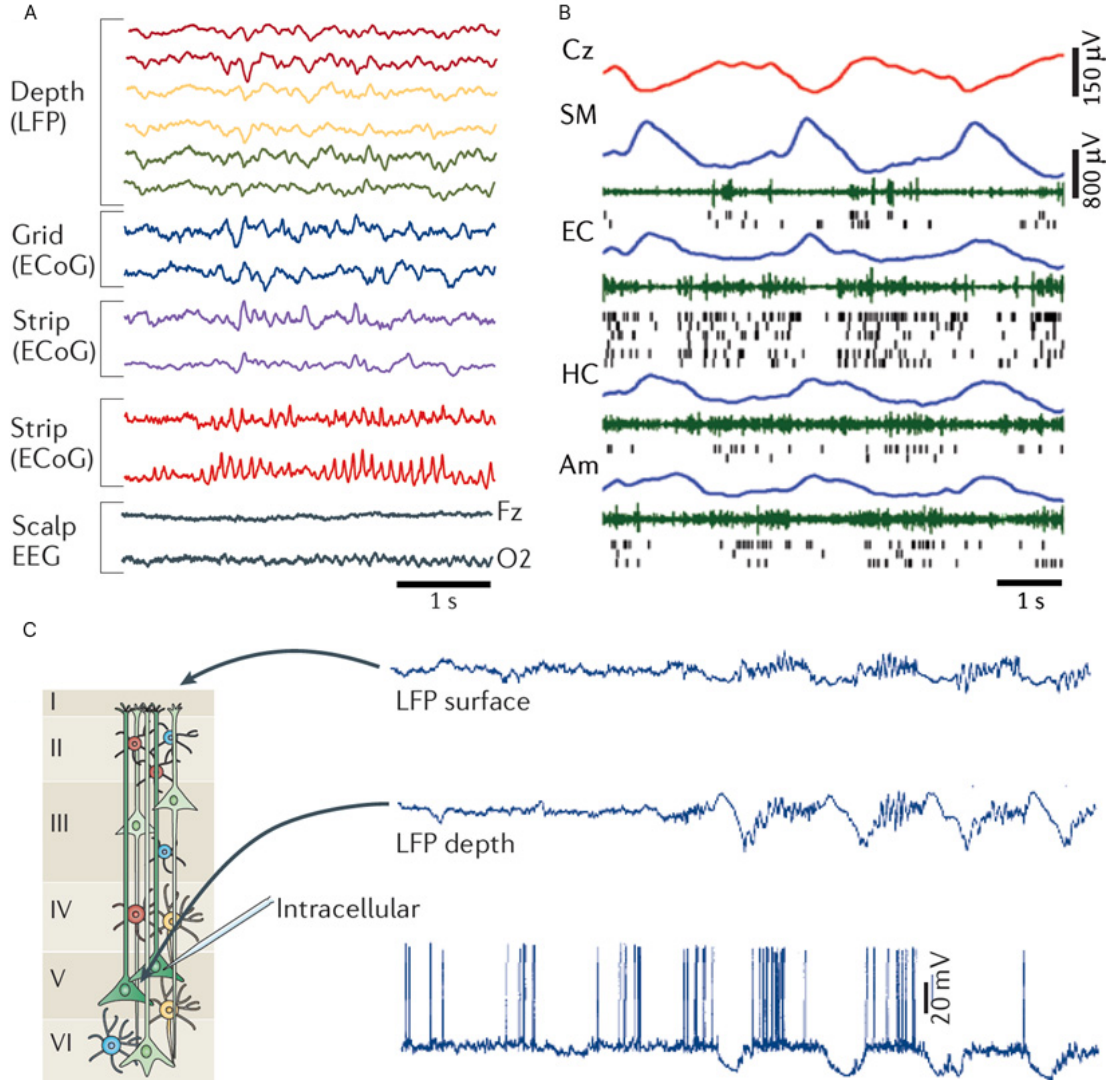


Figure 1.1: Extracellular traces from different recording methods: A) Recordings from three different types of electrodes (EEG, ECoG and LFP) in the left amygdala and hippocampus to measure the local field potential (LFP). B) Recording of slow waves for a 6-second epoch captured by scalp EEG (Cz, red) and LFP using depth electrodes in the supplementary motor area (SM), entorhinal cortex (EC), hippocampus (HC), and amygdala (Am). Additionally, multiple-unit activity is shown in green and spikes of isolated neurons in black. C) Simultaneously recorded LFP traces from the superficial ('surface') and deep ('depth') layers of the motor cortex in an anaesthetized cat and an intracellular trace from a layer 5 pyramidal neuron. The figure is adapted from (Buzsáki et al., 2012)

(LFP). Figure 1.1 C illustrates the comparison between surface and depth LFPs, and figure 1.1 A shows the comparison of EEG, ECoG (electrocardiography) and depth LFP signals. LFPs, generated by the activity of neurons in proximity to an electrode, offer valuable insights into brain function and are often correlated and coupled with MUA (Burns et al., 2010). Figure 1.1 B shows LFP, MUA, and spikes recorded simultaneously from the same sites. Interpreting LFPs is more challenging than MUA, as it involves considering various factors such as the geometry of neurons, sub-threshold neuronal activity, distant sources, and

volume conduction (Buzsáki et al., 2012; Herreras, 2016; Einevoll et al., 2013). Therefore, it is essential to recognize the complexity of these signals, as they reflect a multitude of brain physiological processes.

The structure of neurons is among the top factors affecting LFPs. The production of local field potentials (LFPs) in neurons is significantly affected by their morphology, synapse placement, and electrode recording location (Einevoll et al., 2013). This fact is also supported by computational modelling (Mainen and Sejnowski, 1996; Lindén et al., 2010).

It is believed that the so-called open-field structure neurons contribute more to LFP than closed-field configuration (Einevoll et al., 2013). Open-field neurons have a greater distance between the input and output, resulting in a dipole characterized by different charges on opposite ends. Pyramidal cells are a prime example of such neurons, as they are lengthy and extend across multiple cortical layers, creating strong dipoles. In contrast, closed-field neurons are more symmetrical and extend less across layers, with satellite cells being a good example (Buzsáki et al., 2012). In Figure 1.2 A and B, you can observe the LFP produced by pyramidal neuron models located at different sites around the neuron. In Figure 1.2 C and D - LFP produced by satellite cells models.

Another factor that is worth considering when analyzing LFPs is volume conduction in the brain tissue. Volume conduction refers to the spread of electrical potentials or signals through the conductive medium of the brain tissue. It occurs when an electrical signal generated at one location in the brain spreads to nearby regions through the conductive properties of the tissue (Kajikawa and Schroeder, 2011). This means that the LFP recorded at a specific location may not solely reflect the activity of that particular region but can also include contributions from other regions. It also suggests that the LFP signal recorded at a specific location can be a mixture of signals from multiple sources. All of this makes it harder to understand LFP signals.

1.3 Brain Waves

Hans Berger's initial measurement of brain electrical activity revealed that it was not random fluctuations, but rather brain waves with distinct frequencies (Berger, 1938). This is now known as oscillatory activity in the brain and can be observed in LFP recordings. It plays a significant role in cognitive processes like perception, attention, and memory (Friston et al., 2015).

Oscillations help the brain communicate within and between structures, making neural activity synchronized and timing more precise (Fries, 2015). In the review by Jensen et al. (2019), these oscillations are compared to an audience applauding after a play or a concert. The sound of clapping helps individuals self-organize and synchronize rhythmically without any external organization. This occurs due to communication between individuals through auditory perception. Similarly, neurons in a network also exhibit spontaneous oscillations through synaptic interactions. It could be seen from multiple perspectives: the oscillations themselves are the phenomena created by the synchronization of neurons, but we also notice that neuronal spiking tends to bind to these oscillations or couple with them (Pesaran et al., 2002), so the wave activity is forcing neurons to fire more and in synchrony with it, thus creating an even stronger wave.

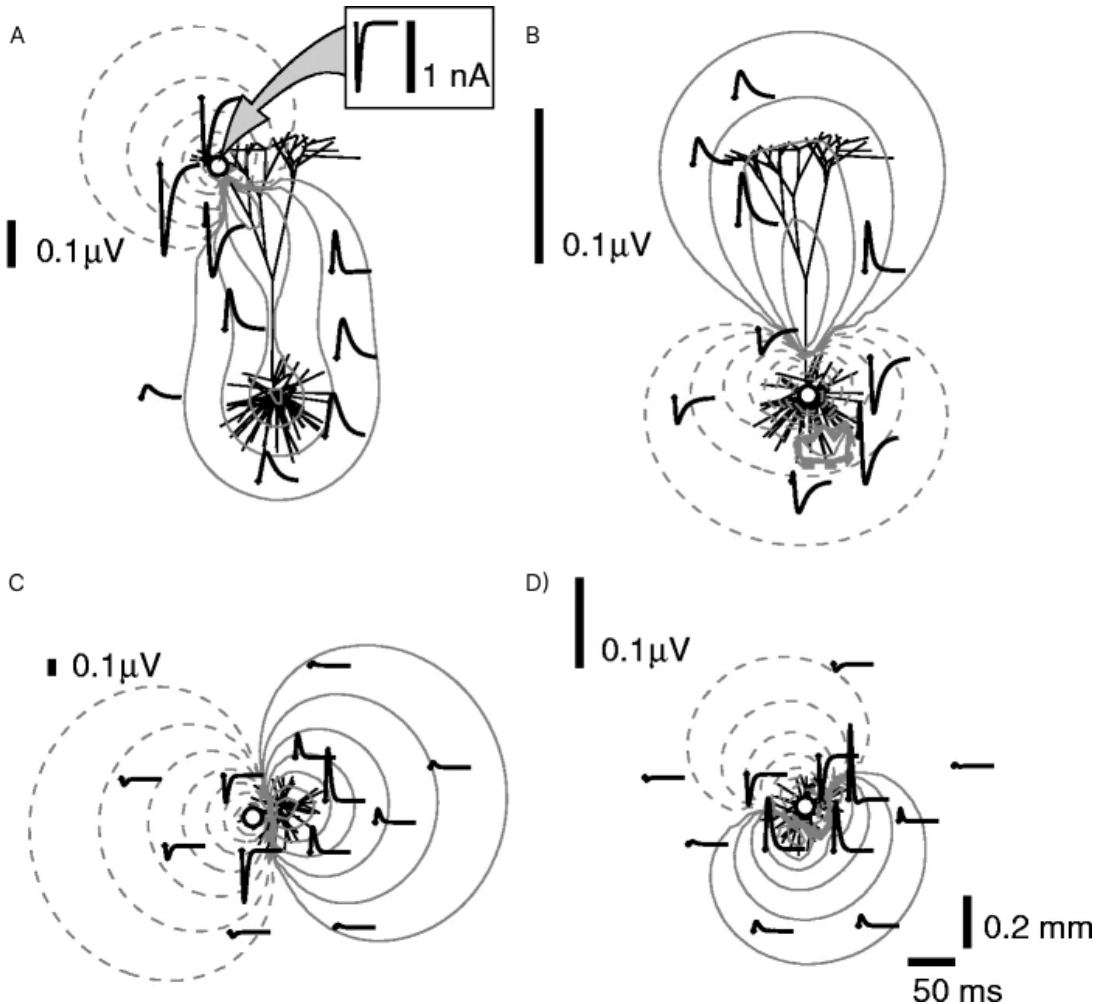


Figure 1.2: Examples of calculated local field potentials (LFPs) that have been modelled after an excitatory synaptic input for various morphological types of neurons. Extracellular potentials are represented by thick solid lines. Grey contour lines show the max LFP amplitudes and decay by a factor of 2 between each contour line. Solid contour lines represent positive LFP values, while dashed lines represent negative values: A) Reconstruction of an L5 pyramidal neuron with an open-field structure and a single excitatory synapse represented by a solid dot on an apical branch. B) Same as A) but with a single excitatory synapse located in the soma. C) Reconstruction of L4 stellate neuron with a closed-field structure and a single excitatory synapse represented by a solid dot on a distal branch. D) Same as C) but with a single excitatory synapse in the soma. The figure is adapted from (Lindén et al., 2010).

Moreover, it has been proven that pacemaker cells exist, and they are responsible for generating certain brain waves, such as theta rhythms in the hippocampus (Kocsis et al., 2022).

Different frequency bands, such as gamma and theta oscillations, are associated with specific cognitive functions. These are the common brain waves:

1. Delta Waves (0.5-4 Hz): Delta waves are the slowest brainwaves. Slow cortical brain waves are those of them that have a frequency below 1 Hz. These waves are a well-established phenomenon and serve multiple functions

within the cortex. They are primarily observed during periods of rest, sleep, or deep anaesthesia (Steriade et al., 1993; Terman et al., 1996).

2. Theta Waves (4-8 Hz): Theta waves are often observed during states of relaxation, daydreaming, and light sleep. They have been linked to memory formation, learning, and creativity (Seager et al., 2002; Winson, 1978; Tesche and Karhu, 2000).
3. Alpha Waves (8-12 Hz): Alpha waves are prominent during wakeful relaxation with closed eyes. These waves were first noticed by Hans Berger in his initial experiments and are commonly referred to as Berger's rhythm (Berger, 1938). Alpha oscillations serve as a default dynamic that the visual brain reverts to when there is no input. Additionally, it is believed that alpha-band oscillations serve as a mechanism for sensory suppression during selective attention, allowing for the filtration of irrelevant sensory information (Foxe and Snyder, 2011).
4. Beta Waves (12-30 Hz): Beta waves are typically observed during active mental engagement, such as focused attention, problem-solving, and decision-making (Jensen et al., 2019). They are associated with cognitive processing, alertness, and concentration.
5. Gamma Waves (30-100 Hz): Gamma waves are the fastest brainwaves and are associated with high-level cognitive functions, including perception, attention, memory, and consciousness (Jensen et al., 2019). During active sensory processing, the gamma band is higher and is believed to be the primary signal responsible for forward input propagation (Bastos et al., 2020).

Furthermore, oscillatory activity in the brain can demonstrate organization in both time and space, which may include the occurrence of travelling waves. These waves move through brain networks and have an impact on neural excitability as they travel (Muller et al., 2018). While travelling waves typically refer to phenomena observed in 2D, it is intriguing to note that observing only one point in space is the same as the usual representation of slow brain waves. Studies have revealed how slow brain waves originating in one cortical area propagate throughout the brain in the form of travelling waves, thus connecting these two concepts (Massimini et al., 2004). Moreover, our understanding of the function of travelling waves closely parallels our knowledge of slow-wave rhythms in the brain. For example, both phenomena have been implicated in memory consolidation during rest (Bhattacharya et al., 2022; Tukker et al., 2020; Miyamoto et al., 2017; Sanchez-Vives, 2020).

During non-REM sleep, a slow oscillation includes a hyperpolarization phase, known as the Down state. During this phase, cortical neurons become hyperpolarized and remain inactive for a few hundred milliseconds. Following the Down state is the depolarization phase, or Up state, which lasts for several hundred milliseconds and is characterized by increased neural activity (Massimini et al., 2004). Various physiological mechanisms contribute to the emergence of these states, such as the blocking of the NMDA receptor in the prefrontal cortex, which seems to impact the occurrence of Up states (Sanchez-Vives, 2020).

In our work, we focused on the Up and Down states as we found that studying them has numerous benefits compared to other methods. However, it's essential to remember the relationship between this concept, travelling waves, and slow-wave rhythm.

1.4 Effects of Anaesthesia on Brain Oscillatory Patterns

There are various types of anaesthesia, and many of them can impact the oscillatory patterns of brain activity. When anaesthesia drugs are administered, they cause changes in the oscillation patterns of brain circuits in specific ways. This can result in a disruption of communication between neurons in different regions of the brain and a loss of consciousness that differs from sleep. The oscillations vary based on the type and amount of anaesthetic used and the age of the patient's brain.

When it comes to cats, the main anaesthetics used in veterinary medicine include ketamine, xylazine, isoflurane, and propofol. These anaesthetics can have different impacts on the oscillatory patterns of brain activity in cats.

1. Ketamine-xylazine anaesthesia: Studies have shown that ketamine-xylazine anaesthesia in cats can reproduce the main features of sleep-related slow oscillation, which are slow, large-amplitude waves in the field potential (Chauvette et al., 2011).
2. Isoflurane anaesthesia: Isoflurane is another commonly used anaesthetic in cats. It has been found to induce slow, delta and alpha oscillations with different patterns compared to propofol (Jiang et al., 2022). The specific impact of isoflurane on oscillatory patterns in cats may vary depending on the depth of anaesthesia.

This suggests that we should carefully consider the used anaesthesia as it may have an effect on our observations.

1.5 On the Anatomy of Primary Visual Cortex

The primary visual cortex, located in the occipital lobe, is a key brain region responsible for processing visual information. It has been mostly studied in cats, macaques, mice, and humans. Although there are some differences between these mammal species, certain main features remain conserved across them. In most mammals, the primary visual cortex is organized into six layers (Samonds and Priebe, 2020). These layers can be clearly distinguished histologically and these layer-to-layer differences are mainly due to the cell composition. Some of these layers may be further subdivided into more sub-layers, but this is already more limited to only certain mammals. Notably, cats have fewer (or less distinguishable) sub-layers compared to primates but they have more (or more distinguishable) than mice (Samonds and Priebe, 2020).

Among the layers of the visual cortex, layer IV is of particular interest because it receives input from the lateral geniculate nucleus (LGN), which in turn

receives input from the retina (Samonds and Priebe, 2020). Cells in this layer are optimized for the primary processing of visual stimuli. Layer IV displays the most pronounced segregation into sub-layers, particularly noticeable in primates. This segregation is supported by histological evidence, as different neuron sub-types are found in each layer, projecting to distinct output layers. Notably, the cat’s primary visual cortex exhibits laminar segregation of inputs from the LGN, similar to macaques and humans as discussed in Samonds and Priebe (2020).

The anatomical differences between cortical layers and sub-layers also indicate functional and connectivity distinctions. In general, the laminar circuitry is organized such that layer IV receives input and performs the fundamental processing of the visual signal as we said above. Then it sends output projections to the superficial layers (located above), which in turn sends the output upstream to other cortical areas or downstream to deep layers (V and VI) in the form of feedback loops (Samonds and Priebe, 2020). This circuitry is a fundamental anatomical feature which enables the complex processing of visual signals.

Another brain area that is discussed in our work is the suprasylvian cortex. This region is related to motor function, higher-order motion processing, visual processing and eye movement convergence (Bando et al., 1996; Hubel and Wiesel, 1969; de Lahunta and Glass, 2009). It is located in the posterior region of the brain, near the primary visual cortex. While the suprasylvian cortex is not precisely related to primary visual processing, it is connected to the primary visual cortex and receives visual information from it (Grant and Shipp, 1991).

The suprasylvian cortex in cats is organized into different regions that are specialized for different functions. The medial bank of the middle suprasylvian sulcus (PMLS) is a region that has been extensively studied and is known to be involved in visual processing. For example, neurons in this region have been found to exhibit visual stimulus selectivity (Price et al., 1988). The lateral suprasylvian cortex (LS) is another region of the suprasylvian cortex that is known to be involved in visual processing (Niida et al., 1997).

In our work, we analyzed signals obtained from the primary visual cortex and the suprasylvian cortex recorded by surface electrodes, as well as intracranial electrodes that were inserted into the cortex to record data from different cortical layers.

1.6 Why to Study Brain at Rest?

We analyzed the activity obtained from the cat’s primary visual cortex and the suprasylvian cortex while the eyes were closed and no active processing was taking place. Readers may ask why it is important to study the brain when it is not doing anything. Specifically, what can we learn from observing the activity in the visual cortex when there are no external stimuli? This question is especially relevant since the primary visual cortex processes visual information. In the absence of such information, one can indeed expect no activity.

But we know that even when the brain is at rest, it is never truly inactive. Resting-state brain activity is spontaneous and displays a remarkable degree of spatial and temporal organization throughout the entire brain (Huang, 2019; Sibert et al., 2022). These patterns of activity form networks that connect regions active during waking, sleeping, and general anaesthesia, known as resting-state

networks. In the visual cortex, it has been demonstrated that these networks are distinct from those found in the brain when awake (Omer et al., 2019).

Research into brain pathologies has shown that these networks' normal activity is a crucial aspect of normal brain function and development (Pizoli et al., 2011). Although the precise function of spontaneous activity in the visual cortex of cats is not entirely clear, it is thought to be essential in establishing proper connectivity in various circuits during brain development. Spontaneous activity in the visual cortex of cats is significant in the development of neural characteristics in the primary visual cortex (V1) (Behpour et al., 2021). For example, computational models have shown that different forms of spontaneous activity can produce a topographic map of neural responses as found in V1 (Erwin et al., 1995; Miikkulainen et al., 2006). Before vision onset in the mouse's primary visual cortex, there are two types of spontaneous activity: local low-synchronicity events from the retina and global high-synchronicity events from the cortex. These spontaneous activity patterns help refine the network between the sensory periphery and the visual cortex. Activity-dependent learning rules translate the properties of these patterns into specific changes in connectivity (Wosniack et al., 2021).

Spontaneous activity in the brain has been shown to predict the survival of developing cortical neurons as shown in Warm et al. (2022). Additionally, Tezuka et al. (2022) has shown that spontaneous activity in the cerebral cortex has been found to contribute to callosal axon projections. Furthermore, spontaneous activity in the brain is believed to be important for maintaining neural plasticity and promoting learning and memory. Studies like Baines and Landgraf (2021) have shown that spontaneous activity in the brain can facilitate the formation of new neural connections and strengthen existing ones.

In summary, even during rest, the brain is far from inactive, exhibiting spontaneous and organized resting-state activity across its entire structure. In the context of the visual cortex in cats, spontaneous activity contributes significantly to neural development and the establishment of appropriate connectivity. Patterns of spontaneous activity in the cortex and retina play critical roles in network refinements between the sensory periphery and the visual cortex during brain development. These findings emphasize the importance of spontaneous activity in understanding brain function and its role in both developmental and fully mature neural circuits.

1.7 The Objective of the Thesis

Surface LFPs play an important role in both medical and research settings, often measured using electroencephalography (EEG) or electrocorticography (ECoG). These LFP signals offer valuable insights into cortical activity without requiring invasive recording techniques. Despite their significance, interpreting these signals remains challenging, partly due to issues like volume conduction (see the introductory part on Volume Conduction for more details 1.2). But partially because little is still known about their origin. Specifically, it is unclear whether the signals solely reflect activity in the superficial layers or if deeper layers also contribute through neuronal projections.

In addition, brain waves (both standing and travelling) are commonly observed and studied on the surface, but their exact origin and propagation path-

ways remain uncertain. The interrelationships between different cortical layers are also not entirely understood.

To address these knowledge gaps, our study focused on analyzing signals from two brain areas in cats during rest: the primary visual cortex and the suprasylvian cortex. We employed two different methods for signal measurement: depth laminar probes and surface electrocorticography (ECoG) electrodes. The depth laminar probes were inserted perpendicularly into the cortex, enabling us to capture signals from various layers within the brain. On the other hand, the surface ECoG electrodes were placed directly on the cortical surface, just beneath the dura mater.

The primary objective of this thesis was to describe neural activity throughout the cortical column during surface events. We particularly focused on local field potential cross-correlations and the structure of the power spectrum across the depth of the cortical column in cats, comparing the results during Up states vs. Down states as measured on the cortical surface. To guide our work, we set specific goals:

1. To examine and compare the LFP signals obtained from ECoG and laminar probes in both the time and frequency domains.
2. To gain insights into the interactions between different cortical layers.
3. To study if brain activity on the surface exhibits any form of spatial structure.

By addressing these goals, we hoped to advance our understanding of brain function in cats and, in turn, contribute to the broader knowledge of neuroscience.

2. Methodology

Our primary objective was to examine the correlation between surface-level electrical activity and cortical activity. We also wanted to investigate the coherence of various frequencies between these signals and explore the potential spatial structure of the surface signal. Additionally, we aimed to resolve differences in activity between channels at varying depths.

Here, we provide a comprehensive overview of the experimental setup and data processing techniques employed in this thesis. Furthermore, we delve into the challenges associated with detecting travelling waves and motivate the analysis of Up and Down states instead. We also explain in detail how these Up and Down states were detected.

2.1 Experimental Setup

The investigation into the relationships between signals involved measuring neural activity from the visual cortex and suprasylvian cortex of anaesthetized cats. The necessary electro-physiological data was provided to us by Diego Contreras (University of Pennsylvania, USA).

Two types of electrodes, namely surface and depth (laminar) electrodes, were utilized to record the neural signals. Surface electrodes were placed directly on the surface of the visual cortex which is known as the electrocorticography (ECoG) technique. Electrocorticography (ECoG) provides higher spatial resolution than electroencephalography (EEG), which records brain activity through electrodes on the scalp. Depth electrodes (laminar) were inserted into the visual cortex and suprasylvian cortex to capture activity from deeper neural layers. Figure 2.1 A provides a visual representation of the experimental procedure. Figure 2.1 B gives an illustration of the laminar organization of a cat's visual cortex.

To ensure unconsciousness during the experiment, the cats were anaesthetized using 1-2% isoflurane. The recordings are referred to as spontaneous because the cat's visual system was not receiving any stimuli.

Simultaneous recordings were made for a continuous 30-minute period using both the depth and surface electrodes. The electrical signals were acquired using a high-resolution recording system with a sampling rate of 20 kHz. These recordings were stored in a digital format for subsequent analysis. Figure 2.1 C shows the example of a recorded signal. The recordings from the suprasylvian cortex were denoted as *w12_18*. The recordings from the primary visual cortex were denoted as *w12_07*.

2.2 Data Preprocessing

The electrophysiological signal is susceptible to line noise, which refers to electrical interference from external sources. This noise can disrupt the recording of electrical signals from cells or tissues. To address the impact of line noise on our analysis, we initially employed a data preprocessing step to remove it from the raw data.

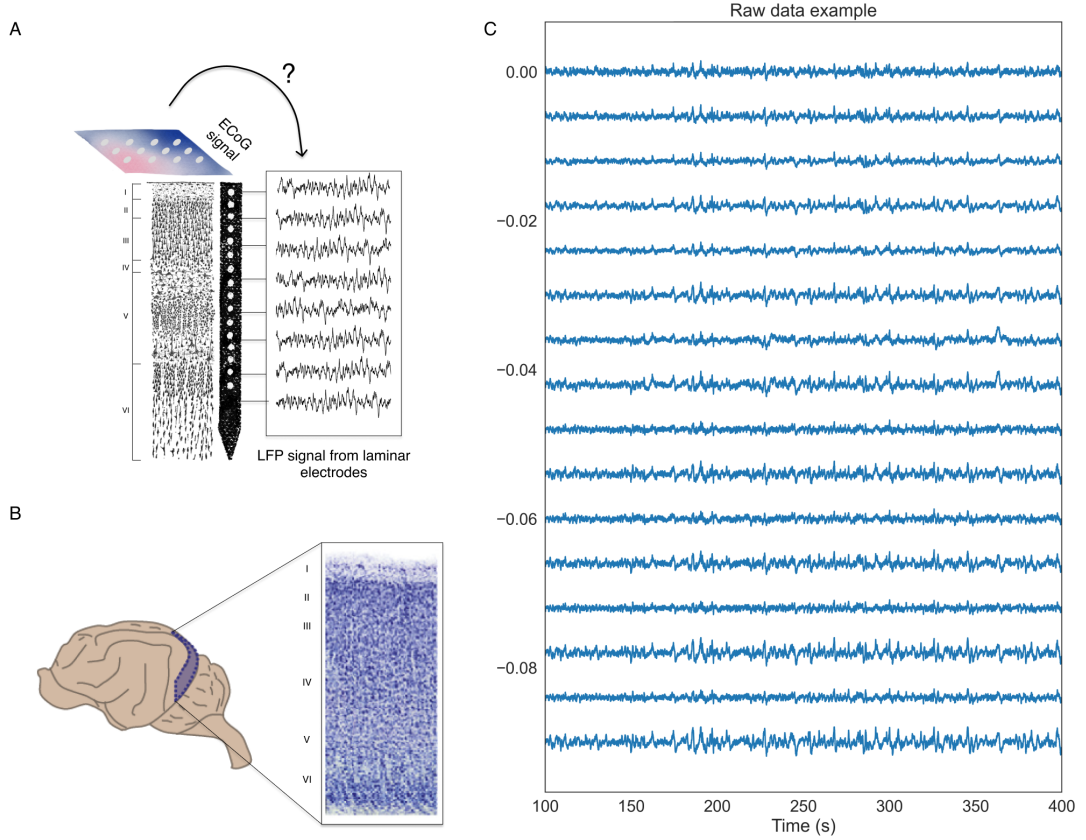


Figure 2.1: Illustration of the experimental setup: A) Simultaneous measurement of electrical signals from a cortical electrode inserted perpendicularly into the cat’s primary visual cortex and from surface electrodes using ECoG (electrocorticography). The experiment aims to investigate potential relationships between these two signals. B) Location and laminar organization of the cat’s primary visual cortex, shown in violet. Adapted from Samonds and Priebe (2020). C) Example of raw LFP signal from the first laminar probe.

To accomplish this, we utilized a notch filter, which selectively attenuates specific frequency bands while preserving others. In our case, we targeted the removal of 60 Hz frequency, as it is commonly associated with line noise in the United States, where the data were collected. This frequency and its harmonics are often indicative of line noise.

By applying the notch filter, we were able to mitigate the effects of line noise on our analysis, enhancing the quality of the data for further investigation and interpretation. However, it is essential to acknowledge that the notch filter does not perform flawlessly and may introduce slight artefacts into the data, as seen in Figure 3.3.

Furthermore, upon observing the data, we identified the presence of a clipping issue. Clipping occurs in digital signal processing when the signal is restricted by the chosen representation’s range. Unfortunately, this issue cannot be rectified through post-processing, but it is crucial to be mindful that some information may be missing due to signal digitization. This clipping phenomenon becomes particularly significant when discussing and observing travelling waves. The limited spatial distinction in signal intensity might lead us to perceive standing waves,

when in fact, they could be a result of value overshoot during signal collection and digitization.

For travelling wave visualization we also employed common reference removal to mitigate the effect of volume conduction, as discussed in Chapter 1.2. The approach for common reference removal is straight forward and included only subtraction of averaged across all channels signal from each channel.

2.3 A Method for Analyzing Surface Events

2.3.1 Exploration of Travelling Waves and Motivation for Up States

As mentioned earlier, travelling waves are oscillatory patterns that exhibit distinct spatial distributions in the brain, with their presence observed on various scales. These waves can traverse the entire brain or occur more locally with spatial resolution in specific regions (Muller et al. (2018)).

However, the study of travelling wave phenomena poses several challenges. A more comprehensive exploration of travelling waves, along with illustrative examples from our data, can be found in the section 3.3. For now, it is important to acknowledge that in our specific case, distinguishing travelling waves from standing waves proved to be challenging. There are several possible explanations for this observation. Firstly, it is plausible that there are no travelling waves present in the data we studied. Alternatively, travelling waves might indeed exist but were not captured due to the scale of our recordings, particularly when considering whole-brain travelling waves that might extend beyond the spatial resolution of local regions.

Another factor that could contribute to our difficulty in identifying travelling waves on the local scale is the clipping issue discussed earlier. This artefact may hinder the observation of travelling waves occurring within the local regions.

Technically, regardless of the presence of travelling waves, our data lack the spatial resolution to precisely determine their spatial relation to our laminar probes.

Nonetheless, we did observe clear "standing" waves in our data at our scale. These waves manifested as ultra-slow oscillatory activity on the surface. To analyze these waves, we aimed to differentiate peaks from negative deflections. We adopted a straightforward approach, considering these peaks as *Up states* and the negative deflections as *Down states*. These states are well-known from the literature as was discussed in Chapter 1.3. In the same section, we also discussed how they are related to travelling waves and slow brain waves. What follows is the more clear description of the detection of these Up and Down states.

2.3.2 Details on Up State & Down State Definition

The ultra-slow fluctuating behaviour of the ECoG signal within the frequency range of approximately 0.5-1 Hz drew our attention for investigation. In our pursuit to characterize this fluctuating behaviour, we opted for a simple and naive approach, defining it as distinct *Up state* and *Down state* regions within the signal.

To isolate the low-frequency component required for this analysis, we applied a lowpass filter, specifically targeting frequencies ranging from 0 to 5 Hz. By filtering the signal in this manner, we aimed to capture the desired ultra-slow fluctuations while minimizing interference from higher-frequency components.

The detection of time intervals for each ECoG channel was performed independently, and subsequently, the detected intervals were merged to define Up states collectively across all channels. This collective definition was motivated by the observation of a high degree of correlation among the channels, as demonstrated in Figure 2.3 B. Among the reasons for this could be the volume conduction phenomenon (already discussed in Chapter 1.2), which could be the case if electrodes did not contact brain tissue well enough.

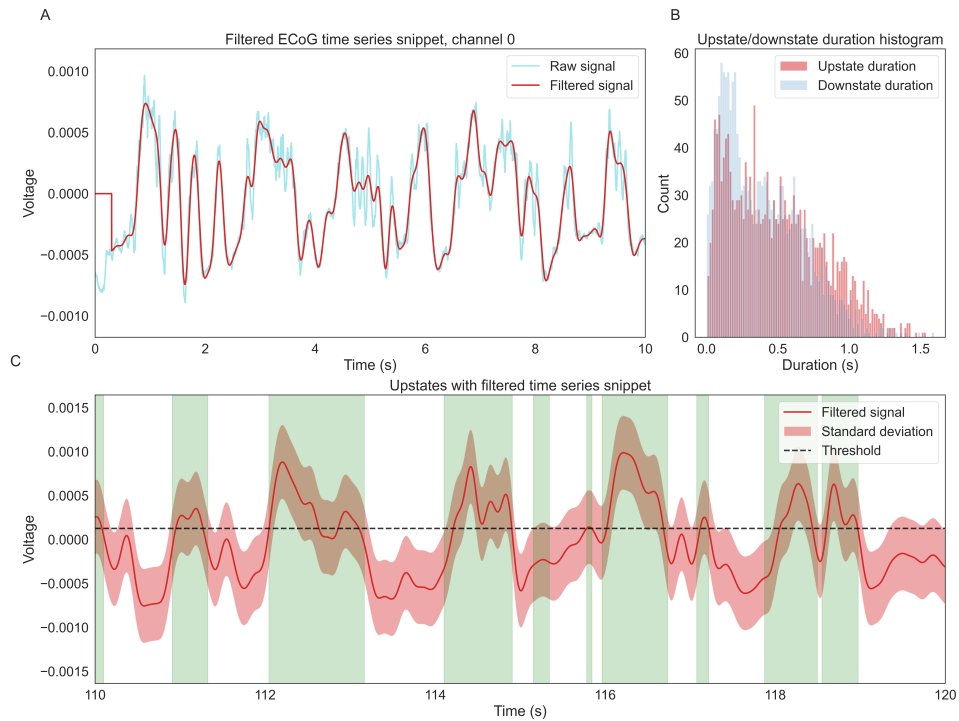


Figure 2.2: Up state detection for experiment *w12_18*. The same figure but for the second recording set is provided in supplementary materials A.1: A) Visualization of lowpass-filtered data. The original (processed) data is depicted in orange, while the blue line represents the lowpass-filtered data. B) Detected Up states are highlighted in green, with the intervals between Up states considered Down states (not highlighted). The dashed black line indicates the voltage threshold used for Up state detection. The light-blue band around the signal represents the standard deviation between channels. C) Histogram displaying the distribution of Up state interval lengths. The green dashed line represents the mean, while the orange line represents the median value.

The identification of Up states was achieved using a thresholding approach. The threshold value was determined according to the following rule:

$$\text{threshold_values} = \text{mean}(\text{data}) + \text{std}(\text{data}) \times \text{threshold_scalar} \quad (2.1)$$

The selection of the threshold scalar was somewhat arbitrary but was supported by careful manual observation of the data. Figure 2.2 C visualizes the threshold value, the data itself, and the overlay of the identified Up states.

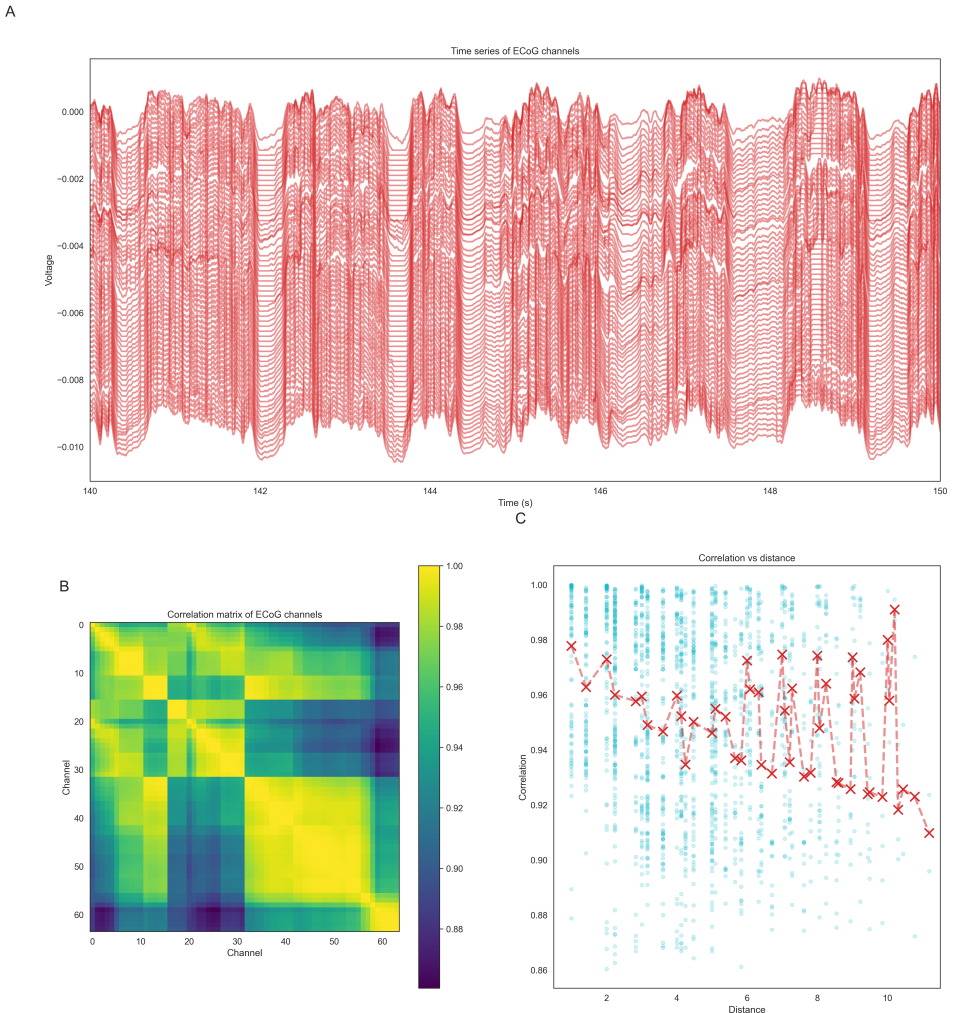


Figure 2.3: ECoG channels analysis for experiment *w12_18*. The same figure but for the second recording set is provided in supplementary materials A.2: A) Visualization of all ECoG channels on a small time interval. B) Heatmap illustrating the Pearson product-moment correlation coefficients computed between each pair of channels. Please note that the spatial proximity of channels is determined by the channel map. C) Heatmap displaying the voltage signal across all channels over a short period of time.

In contrast, Down states were defined as the regions between consecutive Up

states, capturing the transitions from high activity (Up state) to lower activity levels.

Through these steps, we aimed to establish a clear definition of Up states and Down states, enabling further analysis and characterization of the ultra-slow fluctuating behaviour within the ECoG signal.

2.4 Signal to Signal Correlation

Next, we describe the methods used to compute the correlation between different time series in our analysis. The correlation analysis involved measuring the relationship between ECoG channels and the channels of each probe used in the experiment.

To measure the correlation between ECoG channels and the channels of each probe, we utilized the Pearson Correlation Coefficient as implemented in the **Python SciPy library** (the link to the library can be found in Chapter 4). The Pearson Correlation Coefficient measures the linear relationship between two datasets. It varies between -1 and +1, with 0 indicating no correlation. Positive correlations imply that as one variable increases, the other variable increases, while negative correlations imply an inverse relationship.

The Pearson Correlation Coefficient is calculated using the following formula:

$$\rho = \frac{\sum_{i=1}^n (x_i - \bar{x})(y_i - \bar{y})}{\sqrt{\sum_{i=1}^n (x_i - \bar{x})^2 \cdot \sum_{i=1}^n (y_i - \bar{y})^2}} \quad (2.2)$$

where \bar{x} and \bar{y} are the means of the vectors x and y respectively.

For the calculation of ECoG channel-to-channel correlation and probe channel-to-channel correlation, we used the `corrcoef` function from the **Python NumPy library** (the link to the library can be found in Chapter 4). The `corrcoef` function returns the Pearson product-moment correlation coefficients. The resulting correlation matrix contains values between -1 and 1, indicating the degree of correlation between each pair of channels. The correlation matrix was visualized as a heatmap to provide a comprehensive overview of the correlation patterns between channels.

For part of the data, we were interested to analyze the maximum possible correlation between two signals. For that, we computed lagged correlation and found the highest Pearson's Correlation Coefficient for shifted data by respective lag.

2.5 Spectral Analysis

Spectral analysis is a method used to analyze electrophysiology data. Spectral analysis involves breaking down a signal into its component frequencies and analyzing the power of each frequency component. This method is used to identify patterns and changes in the electrical activity of the tissue being studied. There are several different methods of spectral analysis, including the fast Fourier transform (FFT) and autoregressive (AR) methods.

In this thesis, we have used the Welch algorithm for spectral analysis to estimate the power spectrum. The power spectral density (PSD) represents the

distribution of power of a signal across different frequencies. It provides valuable information about the frequency content of a signal.

The Welch algorithm is widely known and available in **Python neurodsp library** (the link to the library can be found in Chapter 4). This is a specific technique used to estimate the PSD from time series data. It is an improvement over the traditional periodogram method, addressing some of its limitations, such as low-frequency resolution and high variance. Welch's method overcomes the limitations of the traditional periodogram by dividing the input signal into overlapping segments and computing a modified periodogram for each segment. The individual periodograms are then averaged to obtain the final PSD estimate. Inside the algorithm, for each windowed segment, a discrete Fourier transform is applied to convert the signal from the time domain to the frequency domain.

Nevertheless, interpreting power spectra obtained by traditional techniques can pose several problems as well shown by Donoghue et al. (2022). The traditional approach of calculating the area under the power spectrum for different frequency bands and considering these values as the power for the respective bands can be problematic because it assumes that the power within a frequency band is uniformly distributed, which is not always the case. This can lead to inaccurate estimates of the power within a given frequency band and can introduce errors in the interpretation of the results. Additionally, this approach does not take into account the aperiodic activity that is present in the power spectrum, which can also affect the accuracy of the estimates.

To overcome these issues in this thesis we have used the **FOOOF library** (the link to the library can be found in Chapter 4) for power density spectra computations. The FOOOF is an algorithm that parameterizes neural power spectra as a combination of an aperiodic component and putative periodic oscillatory peaks (Donoghue et al., 2020). It does not require a priori specification of frequency bands, and it characterizes peaks in the power spectrum in terms of their specific centre frequency, amplitude, and bandwidth. FOOOF assumes all oscillation peaks lie within the fitting range because it does not fit partial Gaussian peaks. This algorithm overcomes the limitations of traditional techniques by separating neural oscillations from aperiodic $\frac{1}{f}$ activity, which contributes some power to all frequencies.

Another way to illustrate the spectral properties of our data that we employed was spectrograms. A spectrogram is a visual representation of the spectrum of frequencies in a signal as they vary over time. It is beneficial compared to PSD because it enables us to also visually observe the temporal variability of spectral properties. The computation of spectrogram is, however, very similar to that of PSD and the already discussed **Python SciPy library** was used by us to calculate it.

2.6 Statistical Testing

Since our data were not normally distributed and did not fulfil the requirement for usual parametric statistical testing, we employed the Mann-Whitney U test in our analysis. The Mann-Whitney U test, also known as the Wilcoxon Rank Sum test, is a non-parametric statistical test used to compare two independent samples or groups (Mann and Whitney, 1947). It is, in general, commonly used

when the data is not normally distributed or when the assumptions of the t-test are not met.

The Mann-Whitney U test assesses whether two sampled groups are likely to derive from the same population or if they have different levels of a variable of interest. It helps determine if there is a significant difference between the two groups. The null hypothesis in the Mann-Whitney U test is that the two populations or groups are equal. In other words, there is no significant difference between them.

The test statistic for the Mann-Whitney U test is denoted as U. It is calculated by summing the ranks for each group and selecting the smaller of the two sums. The value of U can range from 0 to the product of the sample sizes. The Mann-Whitney U test provides a p-value that indicates the probability of obtaining the observed difference between the two groups if the null hypothesis is true. If the p-value was less than 0.001, we assumed it to be a very significant difference (and denoted as ***). We used the implementation provided in the **Python SciPy library** (the link to the library can be found in Chapter 4).

3. Results

3.1 Correlation Analysis of ECoG and laminar Probe Signals

The primary focus of our analysis was to investigate the correlation between signals obtained from electrocorticography (ECoG) and laminar probes (Probe I and Probe II). Note that data were preprocessed with filtering to remove line noise (60 Hz) as was described in Chapter 2.2

First of all, we conducted a cross-correlation analysis of channels on each laminar electrode. The results are depicted in Figure 3.1 A and B. Notably, for both Probe I and Probe II, the upper channels tend to exhibit a negative correlation or no correlation at all with the rest of the channels, while the rest of the channels are highly correlated with each other. There is the same insight from the second experiment that we analyzed. Data can be found in supplementary materials A.3.

Next, we observed that the Up states on the ECoG signal closely mirrored the Up states in the upper channels of Probe II since for the first 200-300 microns the correlation for Probe II is higher than 0.8 as shown in Figure 3.1 C, E. This observation suggests that the upper channels of Probe II are located in close proximity to the brain's surface, resulting in nearly identical activity patterns. In contrast, for the other probe (Probe I), the correlation was less pronounced, and the Up states on the surface did not correspond to the Up states in the upper channels, as depicted in Figure 3.1 C, D, suggesting a slightly different localization of the probe.

An additional observation was the presence of a signal flip in the data, which is likely to be responsible for the flip in PCC values observed in Figure 3.1 C and the pattern of channels' cross-correlation reported in Figure 3.1 A and B. The upper channels exhibit a positive correlation with the ECoG signal but a negative correlation with the deep layers of the cortex. This pattern holds true for both probes, although it is again more prominent in the second probe. The flip could be also seen on the raw signal in Figure 3.1 D and E. Around the middle layers of the cortex, the signal exhibited behaviour similar to the rest but with an opposite sign. This flip can be attributed to the polarity of the neurons and was present in both experiments and both probes, albeit more profoundly in Probe II for both experiments.

We also conducted an investigation into the potential differences in correlation between the surface signal and the cortical signal during Up state and Down state intervals. The findings reveal some interesting insights. The cortical signal exhibits a higher maximum lagged correlation with the surface signal during Down states compared to Up states as shown in Figure 3.2 A. Since we considered the maximum of lagged correlation, the lower correlation in the Up state is not a result of phase shift. Note that lag values (the shift sizes) were small and mostly around 0, which is demonstrated in Figure 3.2 B.

Furthermore, the more positive correlation during Down states holds true across all depths, as depicted in Figure 3.2 C. In the deeper layers of the cortex, the signals start to exhibit a rather negative correlation during Up state.

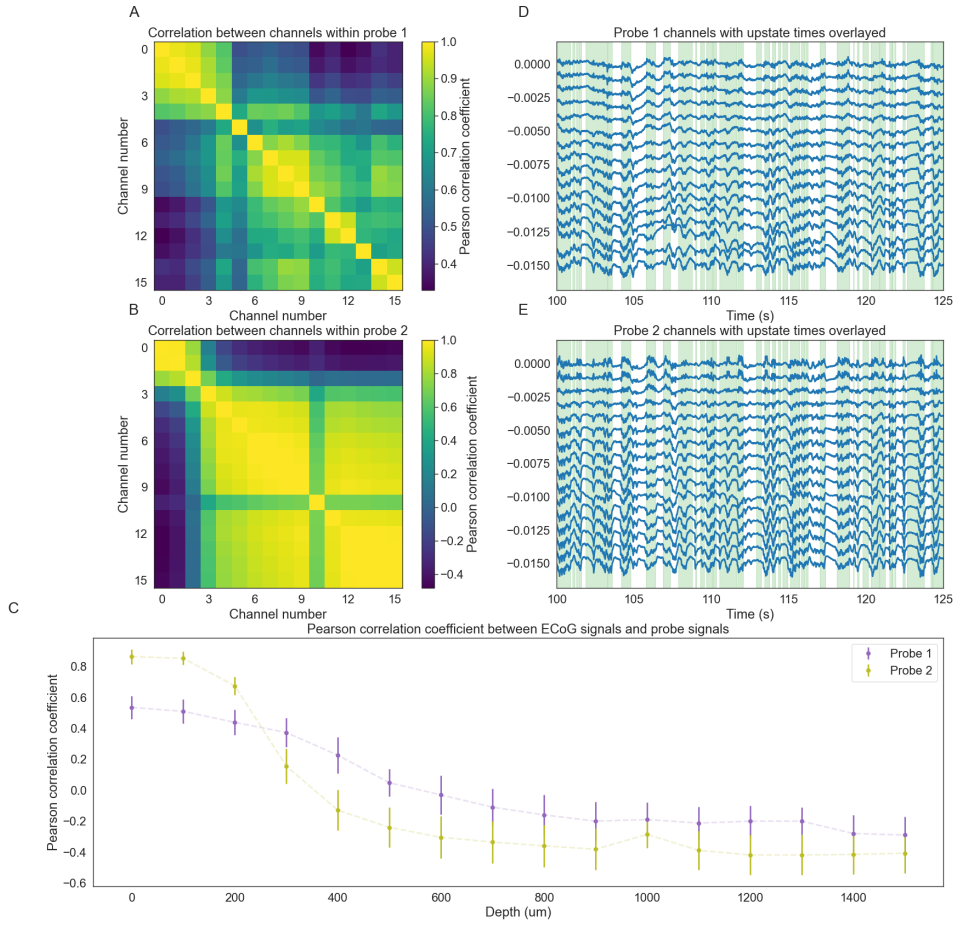


Figure 3.1: Correlation analysis for the primary visual cortex. The same figure but for the suprasylvian cortex is provided in supplementary materials A.3: A) Heatmap illustrating the correlation matrix for channels of Probe I. B) Heatmap depicting the correlation matrix for channels of Probe II. C) Pearson’s Correlation Coefficient that was measured between each ECoG channel and each channel of the probes. The x-axis represents the distance from the surface. Different colours indicate different probes. ECoG channel variation is represented by the standard deviation around the mean of each data point. D) Overlay of Up states from ECoG on Probe I channels. E) Overlay of Up states from ECoG on Probe II channels. Note: Up state timings were determined using the ECoG signal, as described in the Methods section 2.3.2.

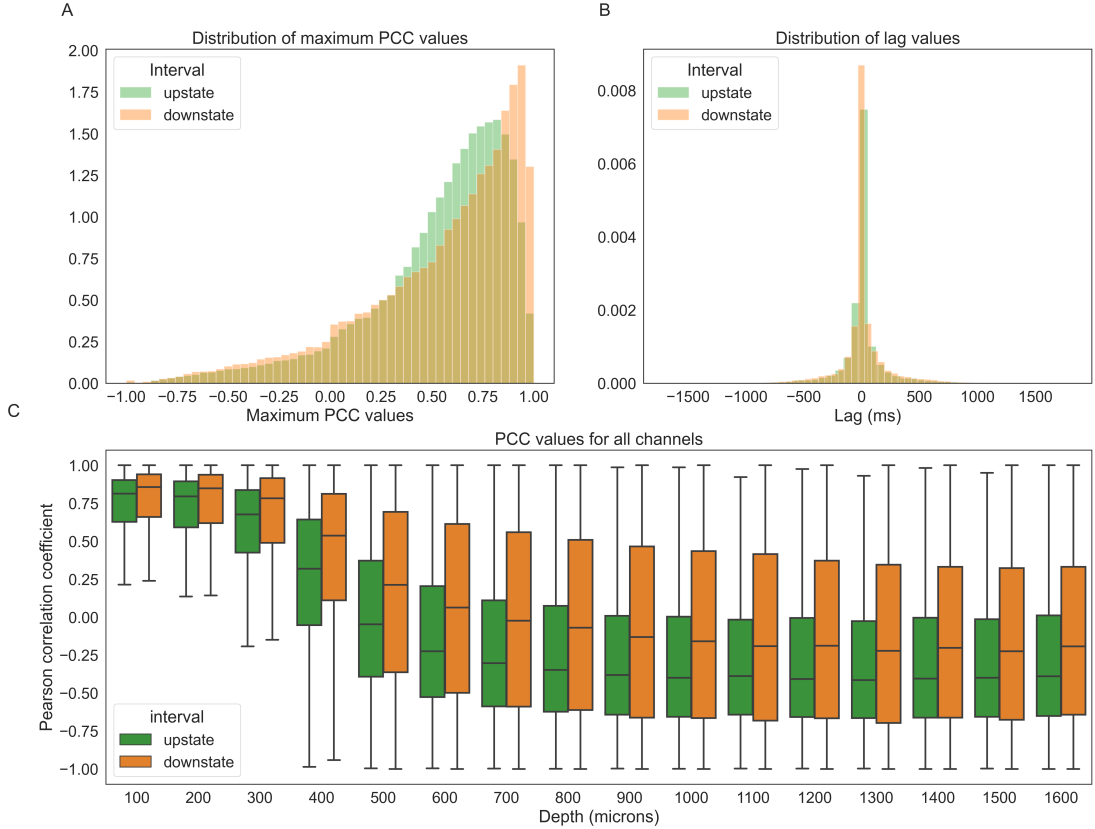


Figure 3.2: Comparison of correlation between two signals during Up state and Down state intervals: A) Normalized histograms showing the maximum correlation for lagged signals. To determine the maximum correlation, we calculate the Pearson correlation coefficient (PCC) for the lag with the highest correlation. Note that if a signal was initially anti-correlated ($PCC < 0$), it was flipped before lagged analysis and maximum PCC computation. Distributions for Up and Down states were significantly different ($p\text{-value} < 0.001$). B) Normalized histograms showing the distribution of lag values used to compute maximum PCC. C) Box-plots representing the correlation coefficient across different probe depths. The x-axis represents the depth of the probe, and the y-axis represents the Pearson correlation coefficient. The data are categorized by boxplots for each depth, summarizing the information for different Up state and downstate intervals. The Up states and Down states are differentiated by colour. This graph combines data from both experiments. For each depth, the difference between the Up and Down states was statistically tested and proved significant ($p\text{-value} < 0.001$).

3.2 Spectral Analysis of Neural Activity During Up States and Down States

3.2.1 Periods of Surface Up States are Characterized by Higher Overall Total Power

Spectral analysis is a method used to analyze time-series data in the frequency domain, rather than the time domain. This involved decomposing the entire signal into various components, represented as waves with different frequencies.

The Power Spectral Density (PSD) is a valuable metric that helps to demonstrate how the power within the signal is distributed across different frequencies. To compute the PSD for each channel, the well-known Welch method was employed, which is described in detail in Chapter 2.5. Another method that we employed to observe spectral properties is a spectrogram. A spectrogram is a visual representation of the frequency content of a signal over time, where the intensity of different frequencies is displayed as a function of time. It is computed using the same method but also visualizes the change in time.

For spectral analysis, we first started by observing the full spectrum of each signal. Then, we specifically explored the spectral characteristics of neural activity during Up state and Down state intervals and analyzed how these spectral characteristics are distributed across different depths of the cortex.

The analysis of the power spectral density of the full signal revealed that there are no prominent oscillations observed in any specific frequency band. Figure 3.3 from A to F demonstrates this finding. It shows the absence of significant oscillatory patterns, except for minimal power observed in the alpha band. This observation held true across all experiments and probes, including both surface and depth electrodes, each shown on the separate graphs from A to F of Figure 3.3. Notably, the different channels on each individual probe exhibited similar spectral behaviours, as depicted by the standard deviation band in Figure 3.3 A to F. For intracranial depth electrodes, it would suggest that there is a low variability in terms of spectral properties among signals from different cortical layers.

Next, we wanted to investigate in better detail what is happening with the signal at the time of Up states. In order to do so, we looked into the raw data in the time domain and its respective spectrogram. In every spectrogram, we observed that there are two types of periods present. One involved minimal power across all bands, and the second was characterized by higher activity broadband. Figure 3.4 B, F and D, H demonstrated this for both experiments and both probes. One could also notice that these periods were highly overlaid with periods of Up states and Down states in raw signals. Interestingly, this also held true for the last channels of deep probes (shown in Figure 3.4 C to H) despite the signal inversion which can be noticed if one compares respective raw signals of ECoG (Figure 3.4 A and E) and last channel of intracranial probes (Figure 3.4 C and H). So the Up states in deep regions were rather overlaid with negative deflections on the signal but were still (similar to ECoG) characterized by higher variance and higher power across broadband.

This motivated us to compare Up states and Down states in terms of their total power. The total power in a Power Spectral Density (PSD) plot represents the overall energy content or variance of a signal across its frequency spectrum. In order to compute that, we ran the Welch algorithm for each interval of Up or Down state across all experiments, probes and channels and for each interval we summed over all powers. We found significant differences between Up state and Down state total power. Figure 3.5 shows that Up states were characterized by higher total power in both surface electrodes (Figure 3.5 A and intracranial electrodes (Figure 3.5 B).

To demonstrate that this finding is non-trivial, we also performed an additional experiment. Before, we worked with Up and Down states detected on the

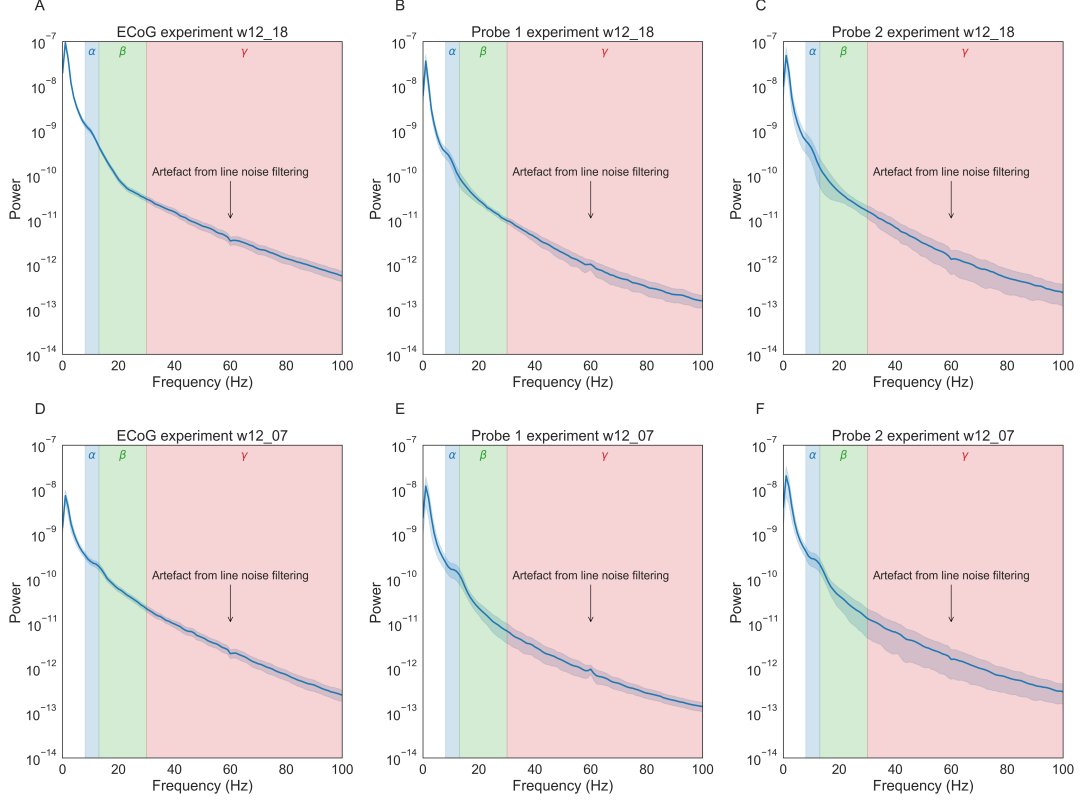


Figure 3.3: Power spectral density (PSD) of the full signal: This figure presents a set of PSD for each experiment and each probe, denoted as A to F. Each sub-figure showcases the mean spectrum of all channels for the respective electrode, with the standard deviation visually represented as the shaded region surrounding the spectral line. To enhance clarity, specific frequency bands of interest are highlighted using distinct colours.

EEG signal. To show that finding holds true only for Up states on the surface we have extracted Up and Down state intervals from the last channels of the intracranial probe and performed the same spectral analysis. This analysis is shown in Figure 3.6 A (for ECOG) and Figure 3.6 B (for intracranial probes). This analysis demonstrated the inverted results with total power prevailing during Down states which is consistent with our general observation of the data flip and the fact that Up states on the surface correspond to the Down states in the deep layers.

3.2.2 The Activity is Dominated by the Alpha and Beta Bands and Demonstrates Depth-Related Variability

We have demonstrated that the power of activity in the primary visual cortex and suprasylvian cortex is closely linked to the defined Up states in this thesis. Now, our focus shifts to two key questions: the presence of specific frequency bands, and the distribution of this activity across the layers of the cortex.

To avoid the mistakes related to the aperiodic component of the spectrum, as discussed in Chapter 2.5, we utilized FOOOF parameterizing approach and

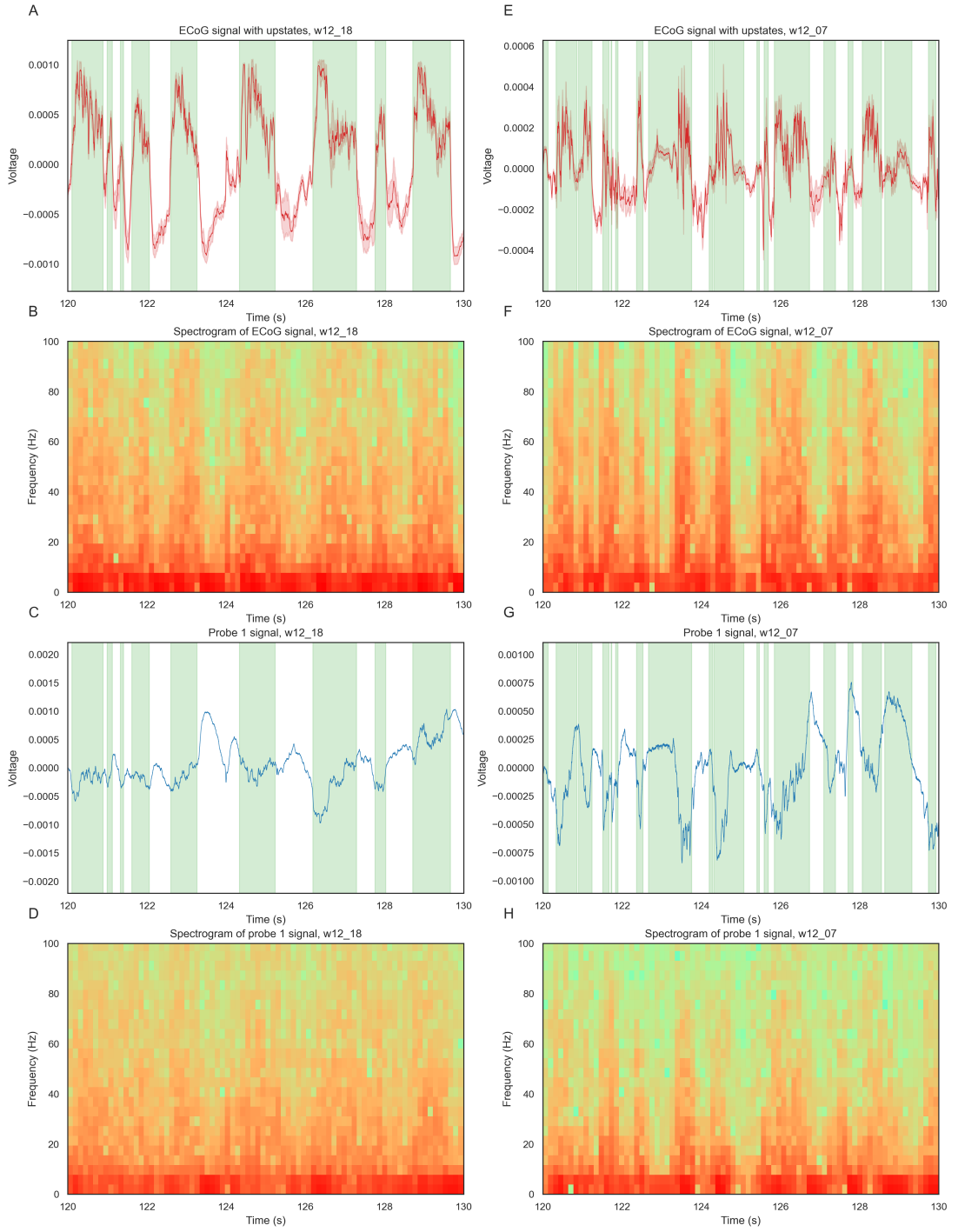


Figure 3.4: Exploring Up states in ECoG Signals: A) ECoG signal from suprasylvian cortex, with green bands highlighting Up state regions. The displayed line represents the average across all channels, while the blue band indicates the standard deviation. B) Spectrogram of the ECoG signal during the same time window. C) Up state regions marked on the last (deepest) channel of Probe 1 from the suprasylvian cortex. D) Spectrogram of the last channel during the same time interval. Sub-figures E) to H) showcase similar data from the primary visual cortex.

reported only centre frequencies of periodic components.

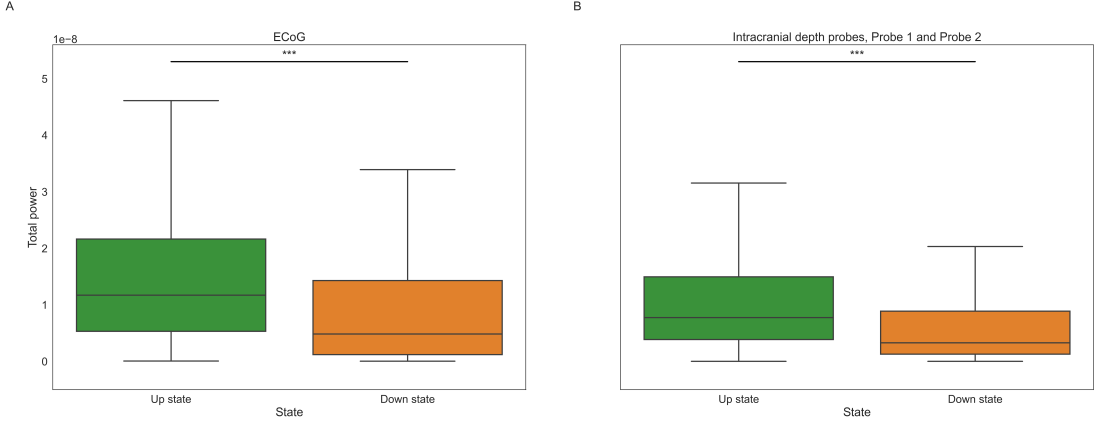


Figure 3.5: Boxplots displaying the total power of Up states and Down states across two experiments. The single y-axis for both plots: A) ECoG probe. B) Probes 1 and 2 (intracranial depth electrodes).

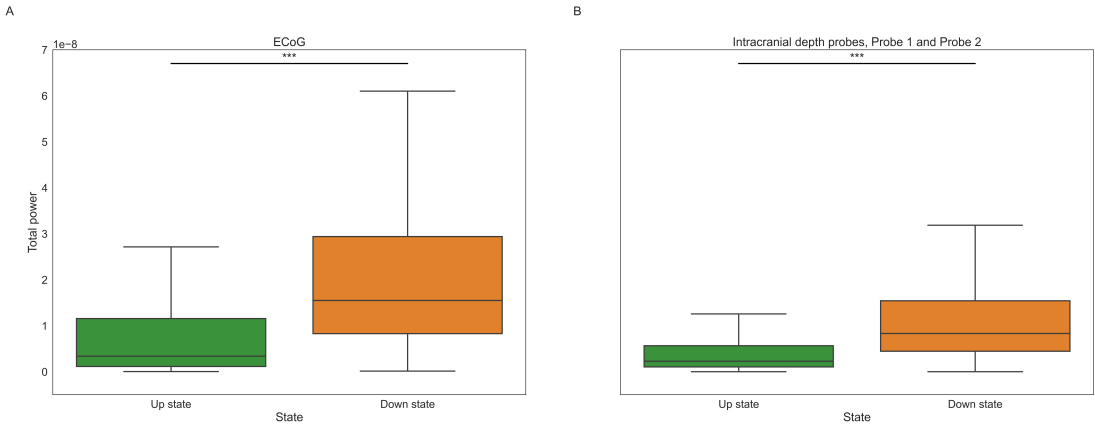


Figure 3.6: Boxplots displaying the total power of Up states and Down states across two experiments with Up and Down states being detected on the last channel of Probe 2. The single y-axis for both plots: A) ECoG probe. B) Probes 1 and 2 (intracranial depth electrodes).

Figure 3.7 A-F indicates that while the activity in some cases is broadband, it predominantly falls within the alpha and beta band, ranging from 8 Hz to 20+ Hz for both experiments.

Our findings reveal that this activity is not uniformly distributed across the layers, as depicted in Figure 3.8 A and B. It is notably less prevalent in the middle layers, around layers II, III, or even IV. Conversely, it appears more prominent in the deep and superficial layers. This discovery may be indicative of modulation by control loops from higher cortical regions, aligning well with known circuitry.

3.3 Travelling Waves

Once we found the alpha and beta band activity inside and on the surface of the cortex, we were intrigued to explore whether this activity exhibits a travelling wave nature. As discussed earlier, the issue of volume conduction complicated the analysis of LFPs (Chapter 1.2). We observed a significant correlation between

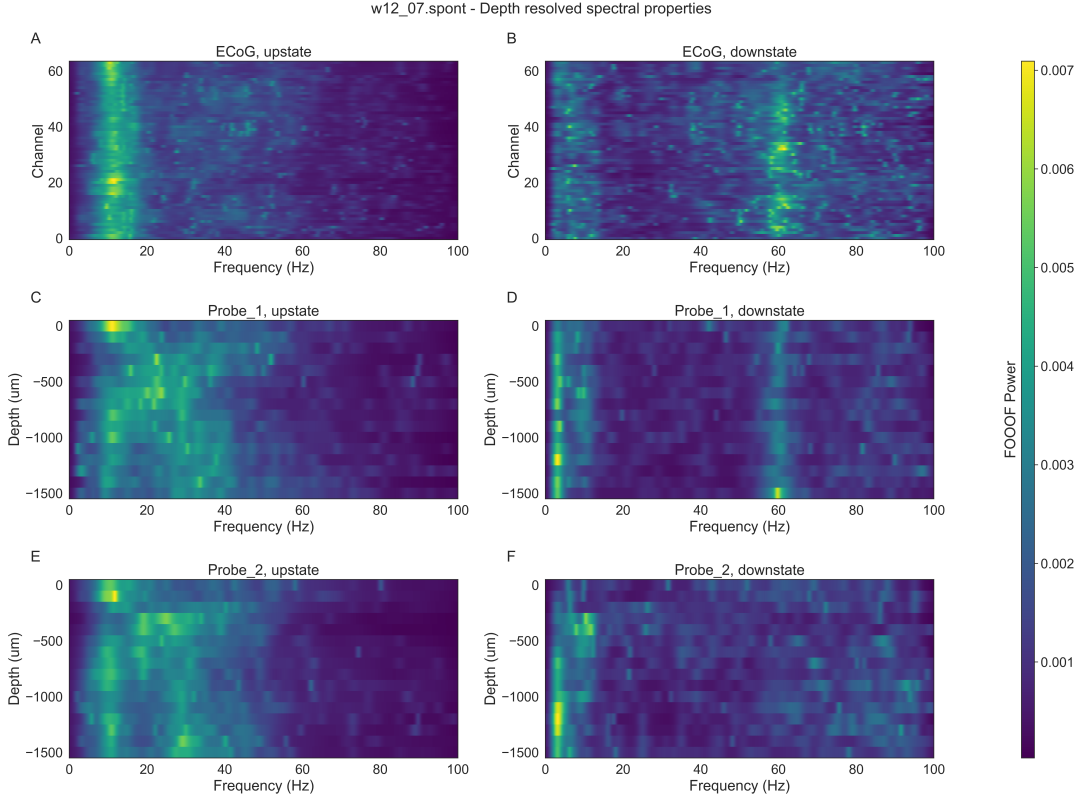


Figure 3.7: FOOOF Spectral Analysis of Up states for recordings from the primary visual cortex. The same figure but for suprasylvian cortex is provided in supplementary materials A.4: A) FOOOF-retrieved power spectra for Up states in the ECoG probe, with the y-axis representing different channels and the x-axis showing various frequencies. C) Similar representation for Up states in Probe 1. E) Corresponding analysis for Up states in Probe 2. Analogously, figures B), D), and F) depict the FOOOF spectral analysis of Down states for the respective probes. On B) and D) 60 Hz artefacts from line noise filtering can be seen.

channels of ECoG (surface electrodes), as depicted in Figure 2.3 B. To address volume conduction, we employed common reference removal, a standard method in electrophysiology that subtracts the average signal from a set of recording electrodes to eliminate common noise sources.

Then to investigate spatial structure in our data for the alpha band, we filtered the alpha band signal in the ECoG channels. Subsequently, we plotted the voltage with respect to its position in the physical space.

Remarkably, our analysis revealed spatially organized alpha-band waves propagating from channels located above to channels situated below, as illustrated in Figure 3.9 with snapshots at different time points. Additionally, we have included a supplementary video for further visualization A.3.

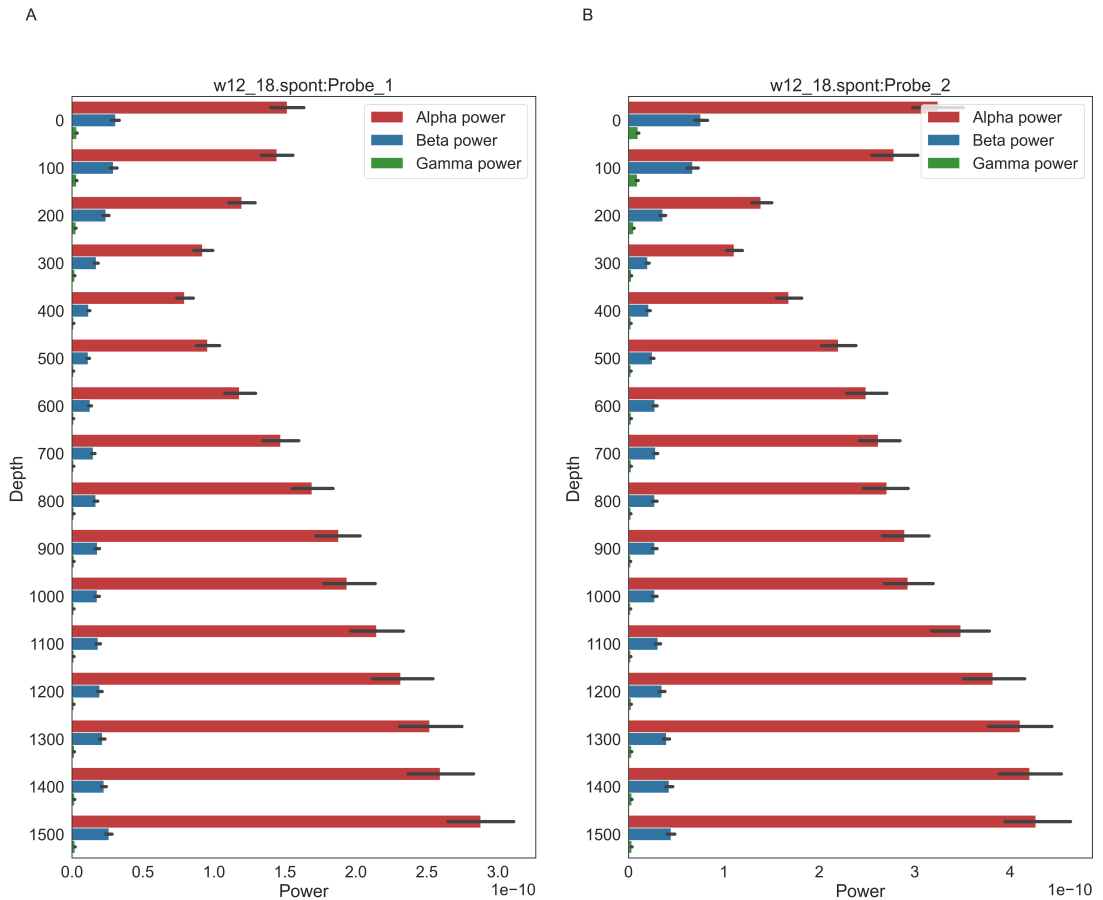


Figure 3.8: Distribution of Power in Alpha, Beta, and Gamma Bands: Bar plots illustrating the power distribution in different frequency bands (alpha, beta, and gamma) across various depths. Sub-figure A) presents data for Probe 1, while Sub-figure B) displays data for Probe 2.

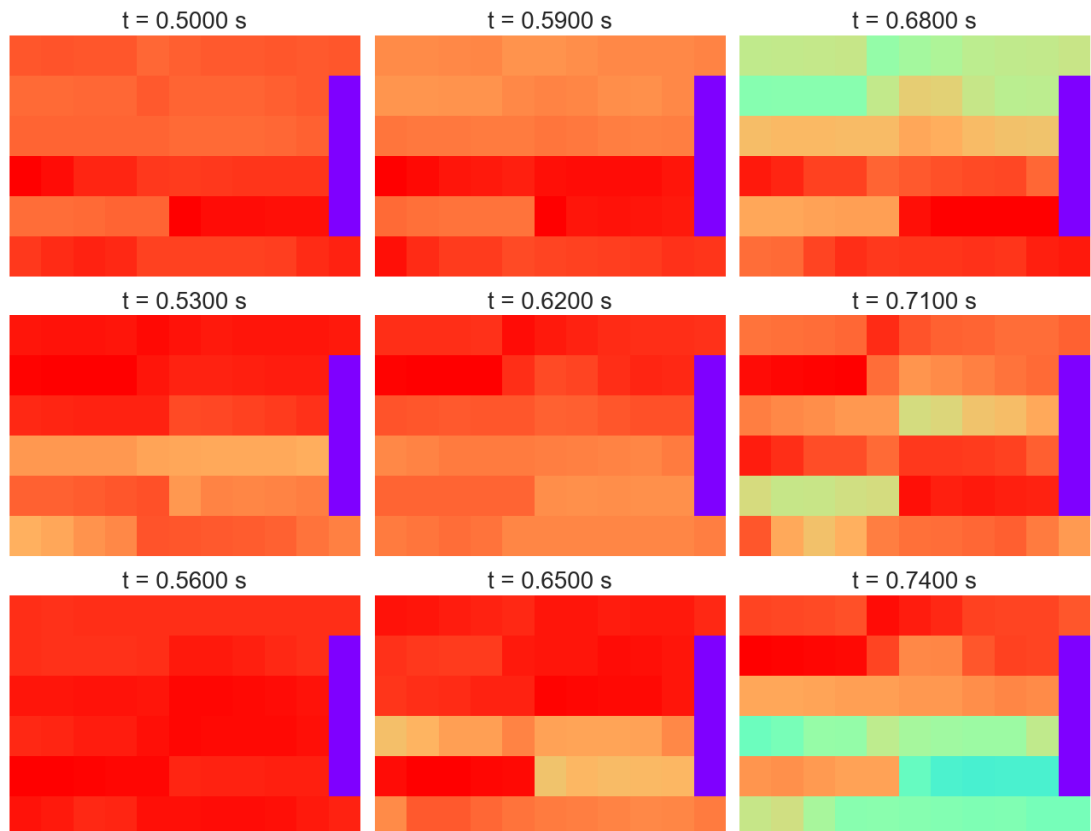


Figure 3.9: Snapshots from spatially localized ECoG channels. The time is indicated above each snapshot. The purple regions on the right are missing channels since the shape of an array was not rectangular.

4. Discussion

In this thesis, we aimed to shed light on how surface local field potentials (LFPs) measured using electrocorticography (ECoG) are related to the signal measured from cortical columns. Specifically, we wanted to investigate whether, during positive deflections on the ECoG signal, which correspond to periods of higher activity, any prominent activity could be seen within the cortex. Additionally, we wanted to explore the spectral properties of surface signals and intracranial signals measured from different layers.

In order to answer posed questions, we relied on data measured using depth laminar probes and surface ECoG electrodes in the primary visual cortex and the suprasylvian cortex of cats. We analyzed the obtained data by first studying the correlation between ECoG channels and depth probes channels, and for each probe, we also investigated correlations between its channels with themselves. What we found is that in general, our data showed a high degree of correlation with surface signal being particularly self-correlated. We also compared measured cross-correlation with regard to the interval and found that cross-correlation was higher during Down states compared to Up states. This is consistent with our next finding that Up states intervals are also characterised by higher total power.

To investigate this further, we employed the method of parameterizing power spectral density proposed by Donoghue et al. (2020). We found that in the primary visual cortex (*w12_18*), the power is dominated by this activity during Up states in alpha/beta bands (10-30 Hz) in the two respective depths (200-500um, 1500um), probably corresponding to layers II-III and layer VI. This is consistent with the fact that the cat had eyes closed and we measured the areas responsible for vision processing (primary visual cortex) and motion processing in vision tasks (suprasylvian cortex). It is still uncertain what is the exact functional significance of the coupling to Up states that we have demonstrated.

Lastly, we attempted to investigate the spatial structure of the surface signal and found that it exhibits some form of spatial non-homogeneity. More analysis, however, would be needed to describe this spatial structure more precisely.

In general, our findings indicate that surface Up states are a reliable indicator of negative deflections and higher total signal variability in deep cortical layers. Since we know that deep cortical layers in the primary visual cortex (V1) participate in the feedback loop, one could assume that the observed activity in the alpha and beta band could be a form of top-down control in the primary visual cortex as, for example, proposed in Bastos et al. (2020). Our findings are also in favour of the belief that pyramidal neurons contribute more to LFPs than stellate cells (Herreras, 2016). In intracranial recordings that we analyzed, we noticed the flip of voltage around negative 300-400 microns. This flip also resulted in deep layers being rather negatively correlated with the ECoG signal, while superficial layers were positively correlated. This also resulted in negative deflections being mostly observed in the deeper layers during surface Up states. This could be easily interpreted as a result of pyramidal neurons' dipole structure.

Throughout this thesis, we have encountered various terms to describe slow brain waves, including ultra-slow oscillations, travelling waves, and Up States. Now, it is time to integrate these concepts and explore the multifaceted nature of

slow cortical brain waves and their functions within the cortex. For our analysis, we utilized averaged across channels one-dimensional signal instead of travelling waves, as this approach enabled a better examination of local-level dynamics. Though, we believe that slow cortical waves are the basic phenomena that we have worked with. They can be decomposed into two components: Up and Down states. This is still an area of active research, but slow brain rhythms have been observed to spread across the brain in the form of travelling waves. These waves facilitate memory and synaptic plasticity, and it is possible that they also interact with other rhythms to facilitate their functioning (Sanchez-Vives, 2020). This finding is also supported by our analysis.

In the future, it would be great to make a more thoughtful analysis of the travelling waves themselves. For example, using more sophisticated methods, such as generalized phase algorithm, proposed by Davis et al. (2019). This algorithm would enable us to study how the phase of the travelling wave on the surface is related to the activity inside the cortical column without the need to detect oscillations, which can be absent. To make this work, we would also require to know the exact position of each channel of ECoG with respect to the intracranial electrode, a piece of information that we did not have this time.

We are also aware of potential issues present in the described analysis. First of all, we suffered from a small sample number. In our study, we analyzed only two recordings obtained from two areas related to vision in cats. To be able to conclude any more robust results, one would require many more samples to analyze. Moreover, we only had access to LFPs from given areas. Having access to MUA would help us better relate observed population-wise activity to specific signals and, thus, would help us to unwind circuitry details and information flow in cortical columns.

We are also aware that several aspects have affected our signals. For example, in our work, 1-2 % isoflurane was utilized as the anaesthetic agent. The effects of this anaesthetic on a cat's visual cortex during rest periods without stimulation are not well-researched. However, some previous studies suggested that isoflurane does have an impact on the spectral properties of spontaneous neuronal activity (Jiang et al., 2022). It is important to consider how different levels of anaesthesia affect the properties of Up and Down states. According to a study using ketamine/medetomidine anaesthetics, light anaesthesia has similar characteristics to slow-wave sleep and occupies a small portion of the Up and Down state duration space. However, deeper levels of anaesthesia result in longer periods of both Up and Down states, and reveal a wider range of durations within the slow oscillatory regime (Torao-Angosto et al., 2021). This suggests that the properties of the Up and Down state are influenced by the level of anaesthesia, and this factor should be taken into account. Thus, repeating the analysis on chronic recordings from awake animals would be of high value, particularly with high-channel count probes such as the Neuropixel probes that are becoming available for chronic recordings (Bimbard et al., 2023). This could be also an interesting perspective for the future.

Secondly, a high degree of cross-correlation for ECoG's channels could be an indicator of volume conduction 1.2. While it can be partially mitigated with common reference removal, in the future, it would be great to have access to recordings without this issue.

Conclusion

To conclude, we wanted to investigate the relationships between large population activities that we observe on the surface of the brain when measuring ECoG with LFPs measured directly from the cortical column. We were also interested to learn more about differences in signal properties from within the column since we expect different cortical layers to have different behaviour.

We learned that cortical layers and surface signals both exhibit slow wave behaviour which can be characterised by the presence of two different periods: Up and Down states. Up states are periods of higher general activity which is supported by our finding of higher total power during this period. We also learned that these states are positively correlated between surface and superficial layers and negatively correlated between surface and deep layers. Subsequently, for deep layers, it is Down states which are periods of higher activity. One could use these findings to hypothesize about possible functional connectivity between these regions. More detailed research is, however, still needed to arrive at robust conclusions, including the investigation of spiking activity of neurons.

Moreover, we demonstrated that this activity that contributes to high total power is largely dominated by the alpha and beta band bands. Finally, we showed that this band's activity exhibits a certain level of spatial organization.

Bibliography

- A. Abbott. Neurophysiology: The man who bared the brain, 2015.
- R. A. Baines and M. Landgraf. Neural development: The role of spontaneous activity. *Current Biology*, 31(23):R1513–R1515, 2021.
- T. Bando, N. Hara, M. Takagi, K. Yamamoto, and H. Toda. Roles of the lateral suprasylvian cortex in convergence eye movement in cats. *Progress in Brain Research*, 112:143–156, 1996.
- A. M. Bastos, M. Lundqvist, A. S. Waite, N. Kopell, and E. K. Miller. Layer and rhythm specificity for predictive routing. *Proceedings of the National Academy of Sciences*, 117(49):31459–31469, 2020.
- S. Behpour, D. J. Field, and M. V. Albert. On the role of lgn/v1 spontaneous activity as an innate learning pattern for visual development. *Frontiers in Physiology*, 12:695431, 2021.
- H. Berger. *Das Elektrenkephalogramm des Menschen*. Geschäftsstelle der Deutschen Akademie der Naturforscher, Halle, 1938.
- S. Bhattacharya, S. L. Brincat, M. Lundqvist, and E. K. Miller. Traveling waves in the prefrontal cortex during working memory. *PLoS computational biology*, 18(1):e1009827, 2022.
- C. Bimbard, F. Takács, J. M. Fabre, M. D. Melin, N. O'Neill, M. Robacha, J. S. Street, E. H. van Beest, A. K. Churchland, K. D. Harris, D. M. Kullmann, G. Lignani, M. Carandini, and P. Coen. Reusable, flexible, and lightweight chronic implants for neuropixels probes. *bioRxiv*, 2023. doi: 10.1101/2023.08.03.551752. URL <https://www.biorxiv.org/content/early/2023/08/06/2023.08.03.551752>.
- S. P. Burns, D. Xing, and R. M. Shapley. Comparisons of the dynamics of local field potential and multiunit activity signals in macaque visual cortex. *Journal of Neuroscience*, 30(41):13739–13749, 2010.
- G. Buzsáki, C. A. Anastassiou, and C. Koch. The origin of extracellular fields and currents—eeg, ecog, lfp and spikes. *Nature reviews neuroscience*, 13(6):407–420, 2012.
- S. Chauvette, S. Crochet, M. Volgushev, and I. Timofeev. Properties of slow oscillation during slow-wave sleep and anesthesia in cats. *Journal of Neuroscience*, 31(42):14998–15008, 2011.
- Z. W. Davis, L. Muller, J.-M. Trujillo, T. Sejnowski, and J. H. Reynolds. Spontaneous traveling cortical waves gate perception in awake behaving primates. *bioRxiv*, page 811471, 2019.
- A. de Lahunta and E. Glass. Chapter 8 - upper motor neuron. In A. de Lahunta and E. Glass, editors, *Veterinary Neuroanatomy and Clinical Neurology (Third Edition)*, pages 192–220. W.B. Saunders, Saint Louis, third

- edition edition, 2009. ISBN 978-0-7216-6706-5. doi: <https://doi.org/10.1016/B978-0-7216-6706-5.00008-1>. URL <https://www.sciencedirect.com/science/article/pii/B9780721667065000081>.
- T. Donoghue, M. Haller, E. J. Peterson, P. Varma, P. Sebastian, R. Gao, T. Noto, A. H. Lara, J. D. Wallis, R. T. Knight, et al. Parameterizing neural power spectra into periodic and aperiodic components. *Nature neuroscience*, 23(12):1655–1665, 2020.
- T. Donoghue, N. Schaworonkow, and B. Voytek. Methodological considerations for studying neural oscillations. *European Journal of Neuroscience*, 55(11-12):3502–3527, 2022. doi: <https://doi.org/10.1111/ejn.15361>. URL <https://onlinelibrary.wiley.com/doi/abs/10.1111/ejn.15361>.
- G. T. Einevoll, C. Kayser, N. K. Logothetis, and S. Panzeri. Modelling and analysis of local field potentials for studying the function of cortical circuits. *Nature Reviews Neuroscience*, 14(11):770–785, 2013.
- E. Erwin, K. Obermayer, and K. Schulten. Models of orientation and ocular dominance columns in the visual cortex: A critical comparison. *Neural computation*, 7(3):425–468, 1995.
- J. Foxe and A. Snyder. The role of alpha-band brain oscillations as a sensory suppression mechanism during selective attention. *Frontiers in Psychology*, 2, 2011. ISSN 1664-1078. doi: 10.3389/fpsyg.2011.00154. URL <https://www.frontiersin.org/articles/10.3389/fpsyg.2011.00154>.
- P. Fries. Rhythms for cognition: communication through coherence. *Neuron*, 88(1):220–235, 2015.
- K. J. Friston, A. M. Bastos, D. Pinotsis, and V. Litvak. Lfp and oscillations—what do they tell us? *Current Opinion in Neurobiology*, 31:1–6, 2015. ISSN 0959-4388. doi: <https://doi.org/10.1016/j.conb.2014.05.004>. URL <https://www.sciencedirect.com/science/article/pii/S0959438814001056>. SI: Brain rhythms and dynamic coordination.
- S. Grant and S. Shipp. Visuotopic organization of the lateral suprasylvian area and of an adjacent area of the ectosylvian gyrus of cat cortex: A physiological and connectional study. *Visual Neuroscience*, 6(4):315–338, 1991. doi: 10.1017/S0952523800006568.
- O. Herreras. Local field potentials: Myths and misunderstandings. *Frontiers in Neural Circuits*, 10, 2016. ISSN 1662-5110. doi: 10.3389/fncir.2016.00101. URL <https://www.frontiersin.org/articles/10.3389/fncir.2016.00101>.
- J. Huang. Greater brain activity during the resting state and the control of activation during the performance of tasks. *Scientific reports*, 9(1):5027, 2019.
- D. H. Hubel and T. N. Wiesel. Visual area of the lateral suprasylvian gyrus (clare—bishop area) of the cat. *The Journal of Physiology*, 202(1):251–260, 1969.

- C. Jennings. The neurobiology of morals. *Nature*, 1999. doi: 10.1038/news991021-6. URL <https://doi.org/10.1038/news991021-6>.
- O. Jensen, E. Spaak, and J. M. Zumer. *Human Brain Oscillations: From Physiological Mechanisms to Analysis and Cognition*, pages 1–46. Springer International Publishing, Cham, 2019. ISBN 978-3-319-62657-4. doi: 10.1007/978-3-319-62657-4_17-1. URL https://doi.org/10.1007/978-3-319-62657-4_17-1.
- J. Jiang, Y. Zhao, J. Liu, Y. Yang, P. Liang, H. Huang, Y. Wu, Y. Kang, T. Zhu, and C. Zhou. Signatures of thalamocortical alpha oscillations and synchronization with increased anesthetic depths under isoflurane. *Frontiers in Pharmacology*, 13, 2022. ISSN 1663-9812. doi: 10.3389/fphar.2022.887981. URL <https://www.frontiersin.org/articles/10.3389/fphar.2022.887981>.
- Y. Kajikawa and C. Schroeder. How local is the local field potential? *Neuron*, 72(5):847–858, 2011. ISSN 0896-6273. doi: <https://doi.org/10.1016/j.neuron.2011.09.029>. URL <https://www.sciencedirect.com/science/article/pii/S089662731100883X>.
- B. Kocsis, S. Martínez-Bellver, R. Fiáth, A. Domonkos, K. Sviatkó, D. Schlingloff, P. Barthó, T. F. Freund, I. Ulbert, S. Káli, V. Varga, and B. Hangya. Huygens synchronization of medial septal pacemaker neurons generates hippocampal theta oscillation. *Cell Reports*, 40(5):111149, 2022. ISSN 2211-1247. doi: <https://doi.org/10.1016/j.celrep.2022.111149>. URL <https://www.sciencedirect.com/science/article/pii/S2211124722009585>.
- H. Lindén, K. H. Pettersen, and G. T. Einevoll. Intrinsic dendritic filtering gives low-pass power spectra of local field potentials. *Journal of computational neuroscience*, 29:423–444, 2010.
- Z. F. Mainen and T. J. Sejnowski. Influence of dendritic structure on firing pattern in model neocortical neurons. *Nature*, 382(6589):363–366, 1996.
- H. B. Mann and D. R. Whitney. On a test of whether one of two random variables is stochastically larger than the other. *The annals of mathematical statistics*, pages 50–60, 1947.
- M. Massimini, R. Huber, F. Ferrarelli, S. Hill, and G. Tononi. The sleep slow oscillation as a traveling wave. *Journal of Neuroscience*, 24(31):6862–6870, 2004.
- R. Miikkulainen, J. A. Bednar, Y. Choe, and J. Sirosh. *Computational maps in the visual cortex*. Springer Science & Business Media, 2006.
- D. Miyamoto, D. Hirai, and M. Murayama. The roles of cortical slow waves in synaptic plasticity and memory consolidation. *Frontiers in neural circuits*, 11:92, 2017.
- L. Muller, F. Chavane, J. Reynolds, and T. J. Sejnowski. Cortical travelling waves: mechanisms and computational principles. *Nature Reviews Neuroscience*, 19(5):255–268, 2018.

- T. Niida, B. E. Stein, and J. G. McHaffie. Response properties of corticotectal and corticostriatal neurons in the posterior lateral suprasylvian cortex of the cat. *Journal of Neuroscience*, 17(21):8550–8565, 1997. ISSN 0270-6474. doi: 10.1523/JNEUROSCI.17-21-08550.1997. URL <https://www.jneurosci.org/content/17/21/8550>.
- D. B. Omer, T. Fekete, Y. Ulchin, R. Hildesheim, and A. Grinvald. Dynamic patterns of spontaneous ongoing activity in the visual cortex of anesthetized and awake monkeys are different. *Cerebral Cortex*, 29(3):1291–1304, 2019.
- B. Pesaran, J. S. Pezaris, M. Sahani, P. P. Mitra, and R. A. Andersen. Temporal structure in neuronal activity during working memory in macaque parietal cortex. *Nature neuroscience*, 5(8):805–811, 2002.
- C. E. Pizoli, M. N. Shah, A. Z. Snyder, J. S. Shimony, D. D. Limbrick, M. E. Raichle, B. L. Schlaggar, and M. D. Smyth. Resting-state activity in development and maintenance of normal brain function. *Proceedings of the National Academy of Sciences*, 108(28):11638–11643, 2011.
- D. J. Price, T. J. Zumbroich, C. Blakemore, and D. Whitteridge. Development of stimulus selectivity and functional organization in the suprasylvian visual cortex of the cat. *Proceedings of the Royal Society of London. Series B. Biological Sciences*, 233(1271):123–163, 1988. doi: 10.1098/rspb.1988.0015. URL <https://royalsocietypublishing.org/doi/abs/10.1098/rspb.1988.0015>.
- J. M. Samonds and N. J. Priebe. The primary visual cortex. 2020.
- M. V. Sanchez-Vives. Origin and dynamics of cortical slow oscillations. *Current Opinion in Physiology*, 15:217–223, 2020. ISSN 2468-8673. doi: <https://doi.org/10.1016/j.cophys.2020.04.005>. URL <https://www.sciencedirect.com/science/article/pii/S2468867320300365>. Physiology of sleep.
- M. A. Seager, L. D. Johnson, E. S. Chabot, Y. Asaka, and S. D. Berry. Oscillatory brain states and learning: Impact of hippocampal theta-contingent training. *Proceedings of the national academy of sciences*, 99(3):1616–1620, 2002.
- C. Sibert, H. S. Hake, and A. Stocco. The structured mind at rest: Low-frequency oscillations reflect interactive dynamics between spontaneous brain activity and a common architecture for task control. *Frontiers in Neuroscience*, 16, 2022. ISSN 1662-453X. doi: 10.3389/fnins.2022.832503. URL <https://www.frontiersin.org/articles/10.3389/fnins.2022.832503>.
- M. Steriade, A. Nunez, and F. Amzica. A novel slow ($\downarrow 1$ hz) oscillation of neocortical neurons in vivo: depolarizing and hyperpolarizing components. *Journal of neuroscience*, 13(8):3252–3265, 1993.
- D. Terman, A. Bose, and N. Kopell. Functional reorganization in thalamocortical networks: Transition between spindling and delta sleep rhythms. *Proceedings of the National Academy of Sciences*, 93(26):15417–15422, 1996. doi: 10.1073/pnas.93.26.15417. URL <https://www.pnas.org/doi/abs/10.1073/pnas.93.26.15417>.

- C. Tesche and J. Karhu. Theta oscillations index human hippocampal activation during a working memory task. *Proceedings of the National Academy of Sciences*, 97(2):919–924, 2000.
- Y. Tezuka, K. M. Hagiwara, K. Ohki, T. Hirano, and Y. Tagawa. Developmental stage-specific spontaneous activity contributes to callosal axon projections. *eLife*, 11:e72435, aug 2022. ISSN 2050-084X. doi: 10.7554/eLife.72435. URL <https://doi.org/10.7554/eLife.72435>.
- M. Torao-Angosto, A. Manasanch, M. Mattia, and M. V. Sanchez-Vives. Up and down states during slow oscillations in slow-wave sleep and different levels of anesthesia. *Frontiers in Systems Neuroscience*, 15, 2021. ISSN 1662-5137. doi: 10.3389/fnsys.2021.609645. URL <https://www.frontiersin.org/articles/10.3389/fnsys.2021.609645>.
- J. J. Tukker, P. Beed, D. Schmitz, M. E. Larkum, and R. N. S. Sachdev. Up and down states and memory consolidation across somatosensory, entorhinal, and hippocampal cortices. *Frontiers in Systems Neuroscience*, 14, 2020. ISSN 1662-5137. doi: 10.3389/fnsys.2020.00022. URL <https://www.frontiersin.org/articles/10.3389/fnsys.2020.00022>.
- D. Warm, D. Bassetti, J. Schroer, H. J. Luhmann, and A. Sinning. Spontaneous activity predicts survival of developing cortical neurons. *Frontiers in Cell and Developmental Biology*, 10:937761, 2022.
- J. Winson. Loss of hippocampal theta rhythm results in spatial memory deficit in the rat. *Science*, 201(4351):160–163, 1978.
- M. E. Wosniack, J. H. Kirchner, L.-Y. Chao, N. Zabouri, C. Lohmann, and J. Gjorgjieva. Adaptation of spontaneous activity in the developing visual cortex. *eLife*, 10:e61619, mar 2021. ISSN 2050-084X. doi: 10.7554/eLife.61619. URL <https://doi.org/10.7554/eLife.61619>.

List of Other Resources

- Python SciPy library.
- Python NumPy library.
- Python neurodsp library.
- Python FOOOF library.

List of Figures

- | | | |
|-----|--|----|
| 1.1 | Extracellular traces from different recording methods: A) Recordings from three different types of electrodes (EEG, ECoG and LFP) in the left amygdala and hippocampus to measure the local field potential (LFP). B) Recording of slow waves for a 6-second epoch captured by scalp EEG (Cz, red) and LFP using depth electrodes in the supplementary motor area (SM), entorhinal cortex (EC), hippocampus (HC), and amygdala (Am). Additionally, multiple-unit activity is shown in green and spikes of isolated neurons in black. C) Simultaneously recorded LFP traces from the superficial ('surface') and deep ('depth') layers of the motor cortex in an anaesthetized cat and an intracellular trace from a layer 5 pyramidal neuron. The figure is adapted from (Buzsáki et al., 2012) . . . | 3 |
| 1.2 | Examples of calculated local field potentials (LFPs) that have been modelled after an excitatory synaptic input for various morphological types of neurons. Extracellular potentials are represented by thick solid lines. Grey contour lines show the max LFP amplitudes and decay by a factor of 2 between each contour line. Solid contour lines represent positive LFP values, while dashed lines represent negative values: A) Reconstruction of an L5 pyramidal neuron with an open-field structure and a single excitatory synapse represented by a solid dot on an apical branch. B) Same as A) but with a single excitatory synapse located in the soma. C) Reconstruction of L4 stellate neuron with a closed-field structure and a single excitatory synapse represented by a solid dot on a distal branch. D) Same as C) but with a single excitatory synapse in the soma. The figure is adapted from (Lindén et al., 2010). | 5 |
| 2.1 | Illustration of the experimental setup: A) Simultaneous measurement of electrical signals from a cortical electrode inserted perpendicularly into the cat's primary visual cortex and from surface electrodes using ECoG (electrocorticography). The experiment aims to investigate potential relationships between these two signals. B) Location and laminar organization of the cat's primary visual cortex, shown in violet. Adapted from Samonds and Priebe (2020). C) Example of raw LFP signal from the first laminar probe. . . . | 12 |

2.2	Up state detection for experiment <i>w12_18</i> . The same figure but for the second recording set is provided in supplementary materials A.1: A) Visualization of lowpass-filtered data. The original (processed) data is depicted in orange, while the blue line represents the lowpass-filtered data. B) Detected Up states are highlighted in green, with the intervals between Up states considered Down states (not highlighted). The dashed black line indicates the voltage threshold used for Up state detection. The light-blue band around the signal represents the standard deviation between channels. C) Histogram displaying the distribution of Up state interval lengths. The green dashed line represents the mean, while the orange line represents the median value.	14
2.3	ECoG channels analysis for experiment <i>w12_18</i> . The same figure but for the second recording set is provided in supplementary materials A.2: A) Visualization of all ECoG channels on a small time interval. B) Heatmap illustrating the Pearson product-moment correlation coefficients computed between each pair of channels. Please note that the spatial proximity of channels is determined by the channel map. C) Heatmap displaying the voltage signal across all channels over a short period of time.	15
3.1	Correlation analysis for the primary visual cortex. The same figure but for the suprasylvian cortex is provided in supplementary materials A.3: A) Heatmap illustrating the correlation matrix for channels of Probe I. B) Heatmap depicting the correlation matrix for channels of Probe II. C) Pearson's Correlation Coefficient that was measured between each ECoG channel and each channel of the probes. The x-axis represents the distance from the surface. Different colours indicate different probes. ECoG channel variation is represented by the standard deviation around the mean of each data point. D) Overlay of Up states from ECoG on Probe I channels. E) Overlay of Up states from ECoG on Probe II channels. Note: Up state timings were determined using the ECoG signal, as described in the Methods section 2.3.2.	20

- 3.2 Comparison of correlation between two signals during Up state and Down state intervals: A) Normalized histograms showing the maximum correlation for lagged signals. To determine the maximum correlation, we calculate the Pearson correlation coefficient (PCC) for the lag with the highest correlation. Note that if a signal was initially anti-correlated ($PCC < 0$), it was flipped before lagged analysis and maximum PCC computation. Distributions for Up and Down states were significantly different (($p\text{-value} < 0.001$)). B) Normalized histograms showing the distribution of lag values used to compute maximum PCC. C) Boxplots representing the correlation coefficient across different probe depths. The x-axis represents the depth of the probe, and the y-axis represents the Pearson correlation coefficient. The data are categorized by boxplots for each depth, summarizing the information for different Up state and downstate intervals. The Up states and Down states are differentiated by colour. This graph combines data from both experiments. For each depth, the difference between the Up and Down states was statistically tested and proved significant ($p\text{-value} < 0.001$).

21

3.3 Power spectral density (PSD) of the full signal: This figure presents a set of PSD for each experiment and each probe, denoted as A to F. Each sub-figure showcases the mean spectrum of all channels for the respective electrode, with the standard deviation visually represented as the shaded region surrounding the spectral line. To enhance clarity, specific frequency bands of interest are highlighted using distinct colours.

23

3.4 Exploring Up states in ECoG Signals: A) ECoG signal from suprasylvian cortex, with green bands highlighting Up state regions. The displayed line represents the average across all channels, while the blue band indicates the standard deviation. B) Spectrogram of the ECoG signal during the same time window. C) Up state regions marked on the last (deepest) channel of Probe 1 from the suprasylvian cortex. D) Spectrogram of the last channel during the same time interval. Sub-figures E) to H) showcase similar data from the primary visual cortex.

24

3.5 Boxplots displaying the total power of Up states and Down states across two experiments. The single y-axis for both plots: A) ECoG probe. B) Probes 1 and 2 (intracranial depth electrodes).

25

3.6 Boxplots displaying the total power of Up states and Down states across two experiments with Up and Down states being detected on the last channel of Probe 2. The single y-axis for both plots: A) ECoG probe. B) Probes 1 and 2 (intracranial depth electrodes).

25

3.7	FOOOF Spectral Analysis of Up states for recordings from the primary visual cortex. The same figure but for suprasylvian cortex is provided in supplementary materials A.4: A) FOOOF-retrieved power spectra for Up states in the ECoG probe, with the y-axis representing different channels and the x-axis showing various frequencies. C) Similar representation for Up states in Probe 1. E) Corresponding analysis for Up states in Probe 2. Analogously, figures B), D), and F) depict the FOOOF spectral analysis of Down states for the respective probes. On B) and D) 60 Hz artefacts from line noise filtering can be seen.	26
3.8	Distribution of Power in Alpha, Beta, and Gamma Bands: Bar plots illustrating the power distribution in different frequency bands (alpha, beta, and gamma) across various depths. Sub-figure A) presents data for Probe 1, while Sub-figure B) displays data for Probe 2.	27
3.9	Snapshots from spatially localized ECoG channels. The time is indicated above each snapshot. The purple regions on the right are missing channels since the shape of an array was not rectangular. 28	
A.1	Up state detection for the primary visual cortex: A) Visualization of lowpass-filtered data. The original (processed) data is depicted in orange, while the blue line represents the lowpass-filtered data. B) Detected Up states are highlighted in green, with the intervals between Up states considered Down states (not highlighted). The dashed black line indicates the voltage threshold used for Up state detection. The light-blue band around the signal represents the standard deviation between channels. C) Histogram displaying the distribution of Up state interval lengths. The green dashed line represents the mean, while the orange line represents the median value.	44
A.2	ECoG Channel Analysis for the primary visual cortex: A) Visualization of all ECoG channels on a small time interval. B) Heatmap illustrating the Pearson product-moment correlation coefficients computed between each pair of channels. Please note that the spatial proximity of channels is determined by the channel map. C) Heatmap displaying the voltage signal across all channels over a short period of time.	45

A.3 Correlation analysis for experiment <i>w12_18</i> : A) Heatmap illustrating the correlation matrix for channels of Probe I. B) Heatmap depicting the correlation matrix for channels of Probe II. C) Pearson's Correlation Coefficient that was measured between each ECoG channel and each channel of the probes. The x-axis represents the distance from the surface. Different colours indicate different probes. ECoG channel variation is represented by the standard deviation around the mean of each data point. D) Overlay of Up states from ECoG on Probe I channels. E) Overlay of Up states from ECoG on Probe II channels. Note: Up state timings were determined using the ECoG signal, as described in the Methods section.	46
A.4 FOOOF Spectral Analysis of Up states for the suprasylvian cortex: A) FOOOF-retrieved power spectra for Up states in the ECoG probe, with the y-axis representing different channels and the x-axis showing various frequencies. C) Similar representation for Up states in Probe 1. E) Corresponding analysis for Up states in Probe 2. Analogously, figures B), D), and F) depict the FOOOF spectral analysis of Down states for the respective probes	47

List of Abbreviations

1. EEG - Electroencephalography
2. LFP - Local Field Potential
3. MUA - Multiunit Activity
4. ECoG - Electrocorticography
5. PCC - Pearson's Correlation Coefficient
6. AP - Action Potential
7. PSD - Power Spectral Density

A. Attachments

A.1 First Attachment

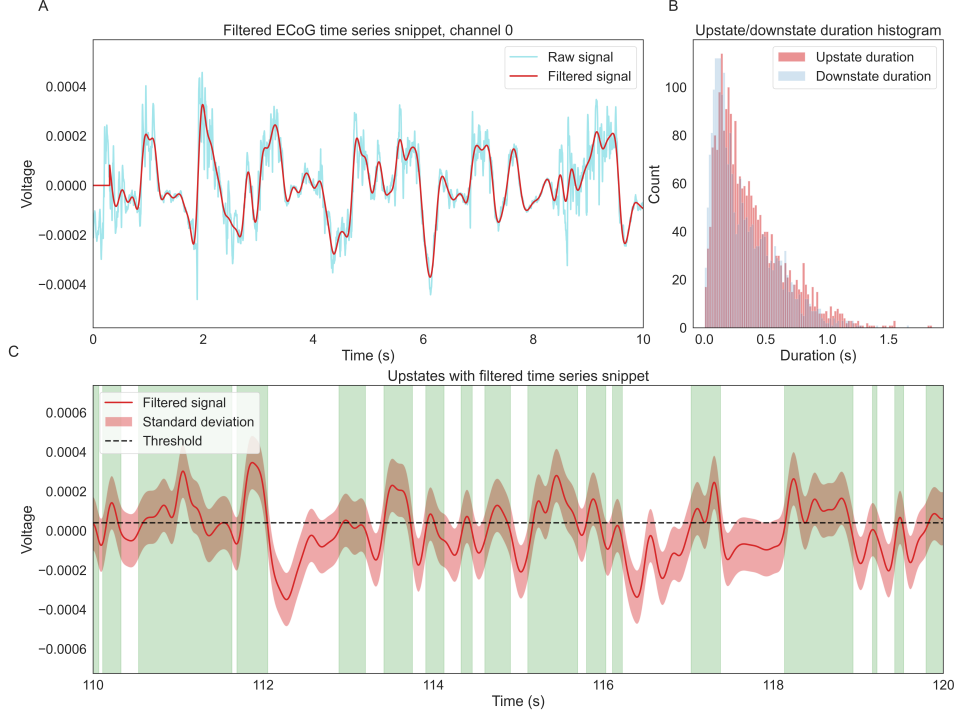


Figure A.1: Up state detection for the primary visual cortex: A) Visualization of lowpass-filtered data. The original (processed) data is depicted in orange, while the blue line represents the lowpass-filtered data. B) Detected Up states are highlighted in green, with the intervals between Up states considered Down states (not highlighted). The dashed black line indicates the voltage threshold used for Up state detection. The light-blue band around the signal represents the standard deviation between channels. C) Histogram displaying the distribution of Up state interval lengths. The green dashed line represents the mean, while the orange line represents the median value.

A.2 Second Attachment

The Python code for the full analysis is available in the GitHub repository.

A.3 Third Attachment

The video illustrating the spatial structure of alpha band activity is available in the same GitHub repository.

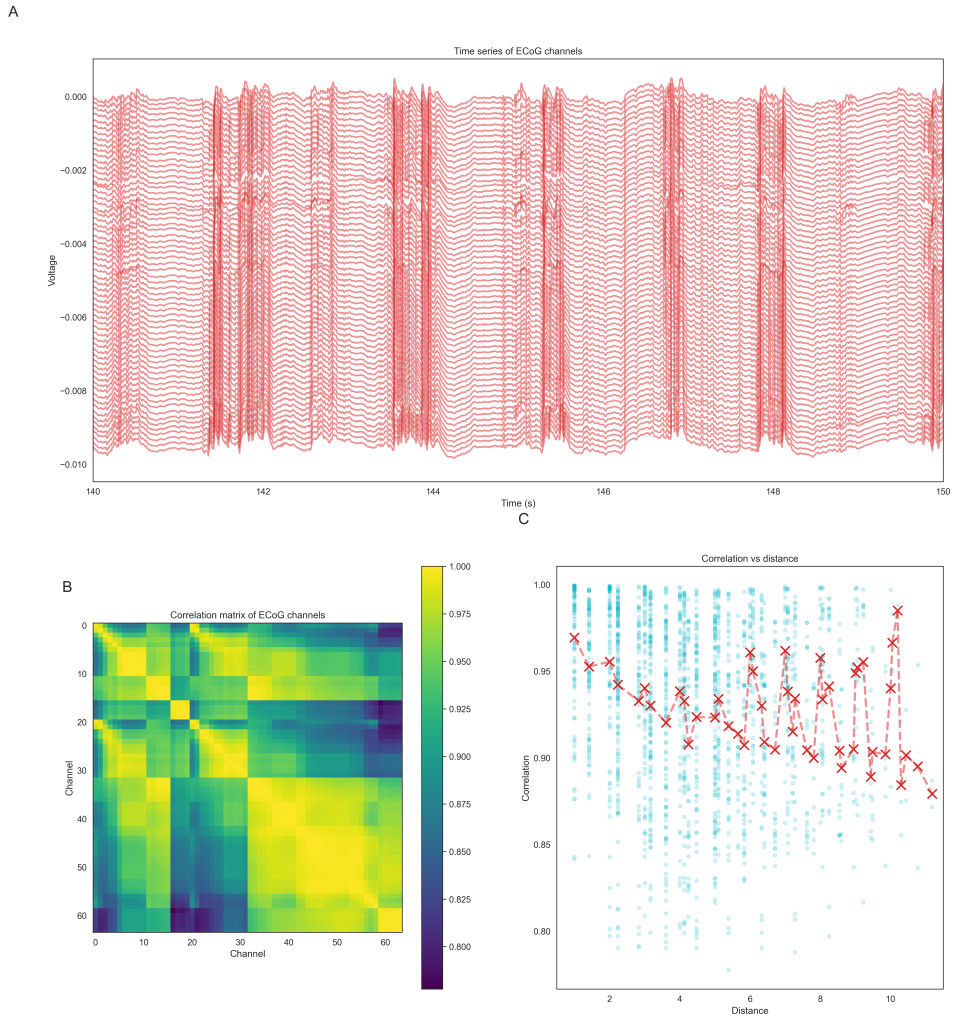


Figure A.2: ECoG Channel Analysis for the primary visual cortex: A) Visualization of all ECoG channels on a small time interval. B) Heatmap illustrating the Pearson product-moment correlation coefficients computed between each pair of channels. Please note that the spatial proximity of channels is determined by the channel map. C) Heatmap displaying the voltage signal across all channels over a short period of time.

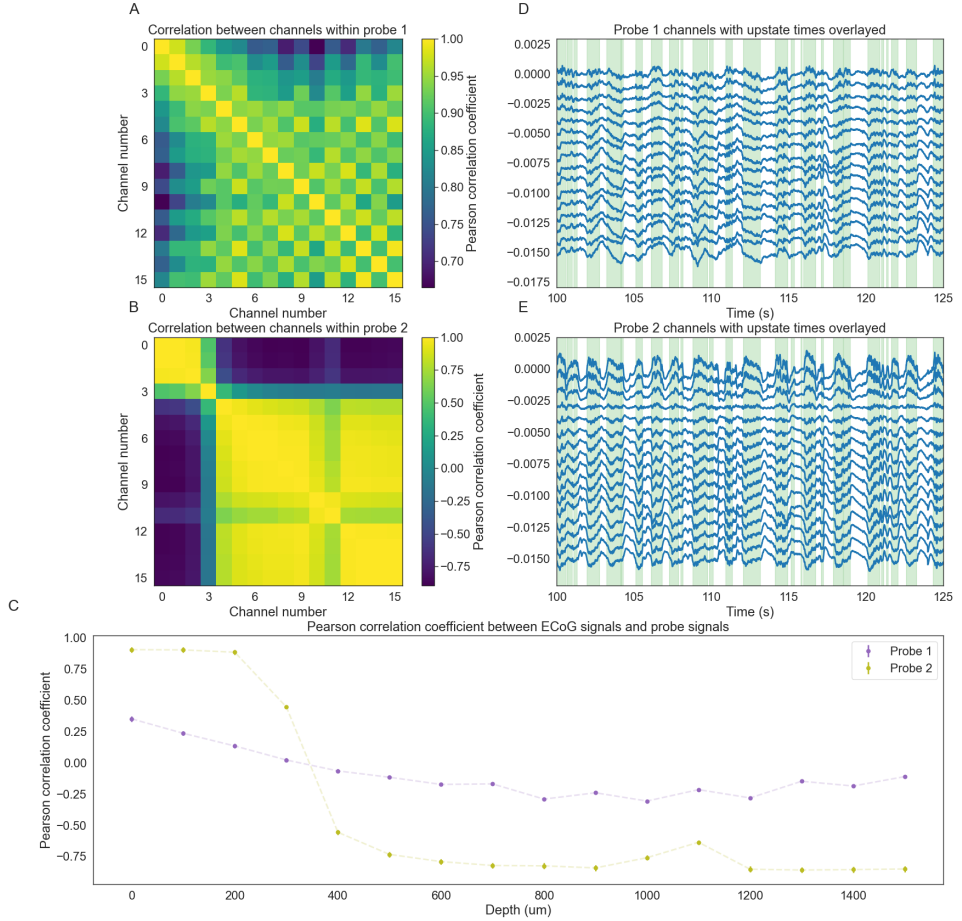


Figure A.3: Correlation analysis for experiment *w12_18*: A) Heatmap illustrating the correlation matrix for channels of Probe I. B) Heatmap depicting the correlation matrix for channels of Probe II. C) Pearson's Correlation Coefficient that was measured between each ECoG channel and each channel of the probes. The x-axis represents the distance from the surface. Different colours indicate different probes. ECoG channel variation is represented by the standard deviation around the mean of each data point. D) Overlay of Up states from ECoG on Probe I channels. E) Overlay of Up states from ECoG on Probe II channels. Note: Up state timings were determined using the ECoG signal, as described in the Methods section.

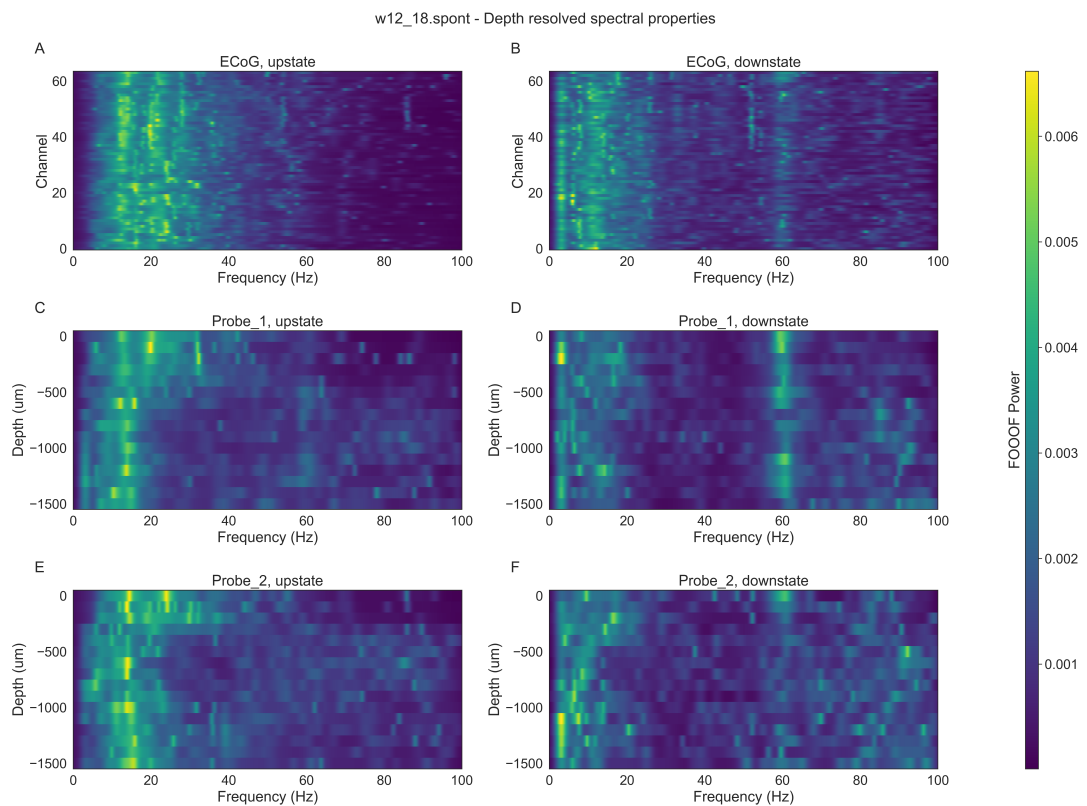


Figure A.4: FOOOF Spectral Analysis of Up states for the suprasylvian cortex: A) FOOOF-retrieved power spectra for Up states in the ECoG probe, with the y-axis representing different channels and the x-axis showing various frequencies. C) Similar representation for Up states in Probe 1. E) Corresponding analysis for Up states in Probe 2. Analogously, figures B), D), and F) depict the FOOOF spectral analysis of Down states for the respective probes